GLIA

WILEY

RESEARCH ARTICLE

Piezo1 channel-mediated Ca^{2+} signaling inhibits lipopolysaccharide-induced activation of the NF-κB inflammatory signaling pathway and generation of TNF-α and IL-6 in microglial cells

Philippa Malko[1] | Xiaoling Jia[1,2] | Ian Wood[1] | Lin-Hua Jiang[1,3,4]

[1]School of Biomedical Sciences, Faculty of Biological Sciences, University of Leeds, Leeds, UK

[2]Key Laboratory of Biomechanics and Mechanobiology (Beihang University), Ministry of Education Beijing Advanced Innovation Center for Biomedical Engineering, School of Biological Science and Medical Engineering, Beihang University, Beijing, China

[3]Department of Physiology and Pathophysiology, and Sino-UK Joint Laboratory of Brain Function and Injury of Henan Province, Xinxiang Medical University, Xinxiang, China

[4]A4245-Transplantation, Immunology and Inflammation, Faculty of Medicine, University of Tours, Tours, France

Correspondence
Lin-Hua Jiang, School of Biomedical Sciences, Faculty of Biological Sciences, University of Leeds, Leeds LS2 9JT, UK.
Email: l.h.jiang@leeds.ac.uk

Abstract

Microglial cells are crucial in maintaining central nervous system (CNS) homeostasis and mediating CNS disease pathogenesis. Increasing evidence supports that alterations in the mechanical properties of CNS microenvironments influence glial cell phenotypes, but the mechanisms regulating microglial cell function remain elusive. Here, we examined the mechanosensitive Piezo1 channel in microglial cells, particularly, how Piezo1 channel activation regulates pro-inflammatory activation and production of pro-inflammatory cytokines, using BV2 and primary microglial cells. Piezo1 expression in microglial cells was detected both at mRNA and protein levels. Application of Piezo1 channel activator Yoda1 induced Ca^{2+} flux to increase intracellular Ca^{2+} concentration that was reduced by treatment with ruthenium red, a Piezo1 inhibitor, or Piezo1-specific siRNA, supporting that Piezo1 functions as a cell surface Ca^{2+}-permeable channel. Priming with lipopolysaccharide (LPS) induced microglial cell activation and production of TNF-α and IL-6, which were inhibited by treatment with Yoda1. Furthermore, LPS priming induced the activation of ERK, p38 MAPKs, and NF-κB. LPS-induced activation of NF-κB, but not ERK and p38, was inhibited by treatment with Yoda1. Yoda1-induced inhibition was blunted by siRNA-mediated depletion of Piezo1 expression and, furthermore, treatment with BAPTA-AM to prevent intracellular Ca^{2+} increase. Collectively, our results support that Piezo1 channel activation downregulates the pro-inflammatory function of microglial cells, especially production of TNF-α and IL-6, by initiating intracellular Ca^{2+} signaling to inhibit the NF-κB inflammatory signaling pathway. These findings reveal Piezo1 channel activation as a previously unrecognized mechanism regulating microglial cell function, raising an interesting perspective on targeting this molecular mechanism to alleviate neuroinflammation and associated CNS pathologies.

KEYWORDS
cytokines, microglia, neuroinflammation, NF-κB, Piezo1

1 | INTRODUCTION

Microglial cells, as innate immune cells of the central nervous system (CNS), play a key role in supporting the function of surrounding neurons (Lannes et al., 2017; Szepesi et al., 2018; Wolf et al., 2017). Under rest conditions, microglial cells tend to assume a highly ramified morphology and continuously survey the CNS tissue with their dynamically motile processes (Davalos et al., 2005). Once activated in response to exposure to pathogen- or danger-associated molecular patterns (PAMP/DAMP), they change to an amoeboid phenotype, aiding motility throughout the CNS and are essential to maintaining homeostatic balance in the neuronal environment (Wolf et al., 2017). Microglial cells have a dual role in mediating CNS responses to tissue infection and injury. Finely coordinated production of inflammatory mediators by microglial and other glial cells is crucial to the regulation of neuroinflammation. The production of pro-inflammatory cytokines is particularly vital in inducing an immune response that promotes phagocytosis of pathogens, dying or damaged cells, and debris (Lannes et al., 2017). Anti-inflammatory signaling originating from microglial cells is also important in downregulating and ultimately resolving the immune response, and promoting CNS tissue repair and remodeling (Orihuela et al., 2016). Chronic and dysregulated production of pro-inflammatory cytokines by microglial cells has, however, been increasingly recognized for its causative link to age-related structural and functional changes in the CNS, particularly the pathogenesis of CNS damage and diseases (Angelova & Brown, 2019; Leng & Edison, 2021; Luca et al., 2018; Sims et al., 2017).

It is well established that microglial cells express intrinsic mechanisms for detecting and responding to diverse chemical signals (Pena-Ortega, 2017). For example, they express the CX3CR1 fractalkine receptor that binds chemokine CX3CL1 produced by neurons (Liu et al., 2015) and the C3a receptor responsible for C3a-induced complement signaling in astrocytes (Wei et al., 2021), both interactions being crucial for bidirectional communications between microglial cells and other cell types within the CNS. Purinergic P2 receptors for extracellular adenosine triphosphate (ATP), released from neurons or glial cells, is another important signaling mechanism for neuron–glial communications (Fields & Burnstock, 2006). In particular, activation of the P2X7 receptor in microglial cells by high concentrations of extracellular ATP released by dying or damaged cells as a DAMP can elicit microglial cell activation (Fields & Burnstock, 2006). Increasing evidence suggests that changes to the mechanical properties of CNS microenvironments, mainly due to aging or various disease conditions, can significantly influence glial cell phenotypes by modulating the activity of mechanosensitive ion channels that convert mechanical signals into intracellular signals (Momin et al., 2021; Velasco-Estevez et al., 2018; Velasco-Estevez et al., 2020). Activation of the Ca^{2+}-permeable Piezo1 channel at the cell surface has emerged as a key molecular mechanism that confers the mechanosensing capacity of diverse cell types (Gudipaty et al., 2017; McHugh et al., 2010; Wang & Xiao, 2018). Recent studies have revealed a vital role for the Piezo1 channel in regulating neuronal differentiation and regeneration in the CNS (Pathak et al., 2014; Song et al., 2019). There is also emerging evidence that Piezo1 is expressed in astrocytes and regulates cytokine production (Velasco-Estevez

et al., 2018; Velasco-Estevez et al., 2020). Particularly, Piezo1 channel activation by Yoda1, a Piezo1-specific activator (Syeda et al., 2015), inhibited the production of interleukin (IL)-1β, IL-6, and tumor necrosis factor (TNF)-α, the major pro-inflammatory cytokines, in astrocytes that were prior primed or activated with lipopolysaccharide (LPS), a PAMP widely used to induce inflammatory responses (Velasco-Estevez et al., 2020). This finding is intriguing, as it strikingly contrasts with other recent studies reporting that Piezo1 channel activation in macrophages, myeloid cells, and nucleus pulposus cells promotes pro-inflammatory responses (Atcha et al., 2021; Solis et al., 2019; Sun et al., 2022). Microglial cells are highly mobile both under physiological and pathological conditions, and able to sense mechanical signals in their microenvironments (Ayata & Schaefer, 2020; Bruno et al., 2021; Davalos et al., 2005). A recent study shows expression of the Piezo1 channel in BV2 microglial cells (Liu et al., 2021). However, the role of the Piezo1 channel in regulating microglial cell function, particularly the production of pro-inflammatory cytokines, is still unknown.

In this study, we investigated the expression of the Piezo1 channel in BV2 cells and primary mouse microglial cells and its role in the regulation of pro-inflammatory responses following LPS-induced microglial cell activation. We further examined the signaling mechanism downstream of Piezo1 channel activation that mediates the regulation of microglial cell function. Our results show that the Piezo1 channel in microglial cells functions as a cell surface Ca^{2+}-permeable channel and mediates Ca^{2+} influx to increase intracellular Ca^{2+} concentration. Importantly, Piezo1 channel activation or, more specifically, Piezo1 channel-mediated Ca^{2+} signaling reduces LPS-induced microglial cell activation and production of TNF-α and IL-6 by inhibiting the NF-κB inflammatory signaling pathway. These findings provide novel insights into the molecular mechanisms regulating the pro-inflammatory phenotype of microglial cells, a functional attribute that is important in maintaining healthy CNS homeostasis under physiological conditions and is also responsible for exacerbating or inducing CNS damage and neurodegenerative diseases.

2 | MATERIALS AND METHODS

2.1 | Chemicals and reagents

All chemicals were purchased from Sigma-Aldrich, unless otherwise specified, and used as per manufacturer's instructions. Solutions were prepared by diluting in deionized water as standard and sterile filtered where appropriate for use in tissue culture.

2.2 | Cell preparation and culture

Murine BV2 cells and primary mouse microglial cells were used in this study. BV2 cells were maintained in Dulbecco's modified Eagle's medium/Nutrient mixture F-12 (DMEM/F12, Gibco) supplemented with 10% fetal bovine serum (FBS, Gibco) at 37°C in a 5% CO_2 atmosphere in a tissue culture incubator. Primary microglial cell cultures were prepared from the brain tissue of 1–3-day old C57BL/6 mouse

neonates. Once sacrificed, brains were extracted, and the meninges and blood vessels removed in Hanks' Balanced Salt Solution (HBSS, Gibco). Isolated tissues were digested in 0.05% trypsin–etheylenediami-netetraacetic acid (EDTA) (Gibco) at 37°C for 20 min before being macerated in DMEM (Gibco), and the resultant suspension filtered through a 40-µm cell strainer. After centrifugation at $300g$ for 5 min, the cell pellet was resuspended in DMEM/F12 supplemented with 10% FBS, 100 units/ml penicillin and 100 µg/ml streptomycin. Cells were seeded in poly-L-lysine-coated 75-cm^2 culture flasks and kept at 37°C in a 5% CO_2 atmosphere. After 3 days in culture, half of the media was removed from the flask and centrifuged at $300g$ for 5 min, and the supernatant collected and supplemented with fresh media, which was used to culture the cells for a further 7–10 days. To isolate microglial cells from the glial bed, flasks were agitated on an orbital shaker for 45 min at 37°C. Detached cells were collected by centrifugation at $160g$ for 5 min, and resuspended in equal parts of the supernatant growth media and fresh culture media before being seeded in different plates as detailed below for experimentation. Immunostaining with an antibody recognizing Iba1, a protein marker for microglial cells, indicates >99% of the cells in our preparations are microglial cells.

2.3 | RNA extraction and RT-qPCR

BV2 cells and primary microglial cells were seeded in six-well plates at 2×10^5 and 5×10^5 cells per well, respectively, and incubated for 24 h prior to use. RNA extraction was carried out using an RNAqueous™-Micro Total RNA Isolation kit (Invitrogen) followed by treatment with a TURBO DNA-free™ kit (Invitrogen) as per manufacturer's instructions. The purity and concentration of RNA were determined using a Nano-drop 2000 spectrophotometer (Thermo Scientific). RNA was reverse-transcribed into cDNA using a High-Capacity RNA-to-cDNA™ kit (Applied Biosystems), and the cDNA stored at −20°C until use. Quantitative polymerase chain reaction (qPCR) was performed using a Quant-Studio™ 3 Real-Time PCR System in 20 µl reactions, each containing 10 ng cDNA, PowerTrack SYBR Green Master Mix (Applied Biosystems) and 400 nM forward and reverse primers. The primer sequences used were as follows: 5'-TCATCATCCTTAACCACATGGTG-'3 (Forward) and 5'-TGAAGACGATAGCTGTCATCCA-'3 (Reverse) for Piezo1 (Zhou et al., 2020), and 5'-CTCGCTTCGGCAGCACA-'3 (Forward) and 5-'AACGCTTCACGAATTTGCGT-'3 (Reverse) for U6, used as a housekeeping gene in microglial cells (Durham et al., 2017). PCR consisted of 95°C for 10 min, 35 cycles of 95°C for 10 s, 55°C for 6 s, and 72°C for 14 s, followed by melt curve analysis from 60°C to 95°C. Data were analyzed using the QuantStudio Design & Analysis Software 2.5.1. PCR products were separated by electrophoresis on a 1% agarose gel and imaged using a Syngene G:BOX Chemi XT4 imager.

2.4 | Western blotting

BV2 cells and primary microglial cells were seeded in six-well plates at 2×10^5 and 7.5×10^5 cells per well, respectively, and incubated for 24 h prior to use. For examining NF-κB activation, cells were treated with 100 ng/ml LPS from *Escherichia coli* O111:B4 alone or with 3 µM Yoda1 (TOCRIS) for 6 or 24 h. Cells were resuspended in sodium dodecyl sulfate (SDS) lysis buffer (10 mM Tris–HCl, 1 mM EDTA, and 1% SDS, pH 8.0) containing a protease inhibitor cocktail (Roche) and samples heated to 95°C for 5 min before the supernatant was collected by centrifugation for 5 min. Lysate protein concentrations were determined using a BCA assay (Thermo Scientific) and diluted using NuPAGE™ 4× lithium dodecyl sulfate (LDS) Sample Buffer (Invitrogen) and distilled water. Protein loading samples were heated at 95°C for 10 min before use, and 20 µg of proteins separated on a 12% SDS-PAGE gel in running buffer (25 mM Tris, 192 mM glycine, and 0.1% SDS) by electrophoresis. Proteins were transferred from the gel to a 0.45-nm nitrocellulose membrane (Whatman) for 90 min at 100 mA using a Trans-Blot® SD Semi-Dry Transfer Cell (BIO-RAD) and transfer buffer (25 mM Tris, 192 mM glycine, and 20% (v/v) methanol). For examining Piezo1 protein expression, cells were lysed in ice cold radioimmunoprecipitation assay (RIPA) buffer (10 mM Tris–HCl pH 8.0, 1 mM EDTA, 1% Triton X-100, 0.1% sodium deoxycholate, 0.1% SDS, and 140 mM NaCl) containing a protease inhibitor cocktail and incubated for 30 min on ice before centrifugation at 11,000g for 20 min at 4°C to collect the supernatant. Samples containing 30 µg of proteins were separated on a 6% SDS-PAGE gel and transferred to a polyvinylidene difluoride membrane (Millipore) for 90 min at 400 mA in transfer buffer (25 mM Tris and 192 mM glycine).

Membranes were blocked in 5% non-fat milk in Tris buffered saline (TBS: 20 mM Tris and 15 mM NaCl, pH 7.2) containing 0.1% Tween-20 (TBST) before being incubated with primary antibodies diluted in TBST and 1% nonfat milk at 4°C overnight. Primary antibodies used were β-actin (C4) at a dilution of 1: 2000 (sc-47,778, Santa Cruz), NF-κB p65 (L8F6) at 1: 500 (6956 S, Cell Signaling Technology), p38 at 1: 500 (9212 S, Cell Signaling Technology), p44/42 (ERK1/2) at 1: 500 (9102 S, Cell Signaling Technology), phospho-NF-κB p65 (Ser536) (93H1) at 1: 500 (3033 S, Cell Signaling Technology), phospho-p38 (Thr180/Tyr182) at 1: 500 (9211 S, Cell Signaling Technology), phospho-p44/42 (ERK1/2) (Thr202/Tyr204) at 1: 500 (9101 S, Cell Signaling Technology), and Piezo1 (extracellular domain) at 1: 500 (15939-1-AP, Proteintech). After washing in TBST, membranes were incubated with corresponding horseradish peroxidase (HRP)-conjugated secondary bovine anti-mouse or anti-rabbit IgG antibodies (Santa Cruz) at 1: 5000 at room temperature for an hour. Membranes were washed in TBST and then TBS before being incubated with an EZ-ECL Enhanced Chemiluminescence Detection Kit (Biological Industries) for detection using a Syngene G:BOX Chemi XT4 imager.

2.5 | Immunofluorescent confocal imaging

BV2 cells and primary microglial cells were seeded on glass coverslips in 24-well plates at 1×10^4 cells and 3.5×10^4 cells per well, respectively. Cells were incubated for 24 h prior to treatment with

100 ng/ml LPS alone or with 3 μM Yoda1 for 24 h. Cells were fixed using Zamboni's fixative solution, made of 15% picric acid and 2% formaldehyde in phosphate buffered saline (PBS), for 45 min at room temperature and washed with PBS. Coverslips were incubated for 1 h at room temperature in a blocking solution (5% goat serum and 2% Triton X-100 in PBS), followed by incubation with the primary anti-body diluted in blocking solution at 4°C overnight. Primary antibodies used were NFAT1 at 1: 50 (4389 S, Cell Signaling Technology), NF-κB p65 (L8F6) at 1: 200 (6956 S, Cell Signaling Technology) and Piezo1 (extracellular domain) at 1: 200 (15939-1-AP, Proteintech). Cells were washed with PBS and incubated with secondary fluorescein isothiocy-anate (FITC)-conjugated goat anti-mouse or anti-rabbit IgG antibodies at 1: 500 (Sigma) for 2 h at room temperature. Cells were washed with PBS, rinsed in water and mounted onto glass microscope slides, using SlowFade™ Gold Antifade Mountant with 4',6-diamidino-2-phenylin-dole (DAPI) (Life Technologies), and imaged using a Zeiss LSM 880 inverted laser scanning confocal microscope.

Analysis of NF-κB p65 and NFAT1 translocation from the cytosol to the nucleus was carried out using ImageJ software and an adapted pro-tocol described in a previous study (Noursadeghi et al., 2008). Briefly, a median filter (3.0 pixel radius) was applied to both the FITC and DAPI stained images to remove noise. An automatic threshold was applied using settings that appropriately captured the cellular or nuclear area and used to generate a binary mask of the image. The DAPI mask repre-senting the nuclear region of interest (ROI) was subtracted from the FITC mask representing the whole cell area to create a mask that represented the cytosolic fraction of cells. The nuclear and cytosolic ROIs were applied to the original FITC image, and quantitative fluorescence data for each image analyzed to give the ratio of nuclear and cytosolic proteins.

2.6 | Measurement of intracellular Ca^{2+} concentration

BV2 cells and primary microglial cells were seeded in poly-L-lysine-coated black 96-well plates (Greiner Bio-One) at 5×10^4 cells per well and incubated overnight. Cells were washed using standard bath solu-tion (SBS: 134 mM NaCl, 5 mM KCl, 8 mM glucose, 10 mM HEPES, 1.2 mM $MgCl_2$, and 1.5 mM $CaCl_2$, pH 7.4) and incubated at 37°C in SBS containing 4 μM Fura-2 AM (Invitrogen) and 0.04% Pluronic™ F-127 (Invitrogen) for 1 h in darkness. Cells were again washed with SBS and maintained in 200 μl SBS per well. For some experiments, extracellular Ca^{2+}-free solution (134 mM NaCl, 5 mM KCl, 8 mM glu-cose, 10 mM HEPES, 1.2 mM $MgCl_2$, and 0.4 mM EGTA, pH 7.4) was used. Fluorescence was alternatively excited at 340 nm and 380 nm and emission at 510 nm measured every 5 sec, using a FlexStation 3 Multi-Mode Microplate Reader (Molecular Devices). Yoda1 was added after 65 sec after establishment of the baseline. In experiments exam-ining Piezo1 inhibitor ruthenium red (RR; Merck), cells were incubated with SBS containing indicated concentrations for 5 min prior to addi-tion of Yoda1. The fluorescence ratio F340/F380, used to indicate the intracellular Ca^{2+} concentration ($[Ca^{2+}]_i$), was plotted using Soft-maxPro software (Molecular Devices).

2.7 | Transfection with siRNA

BV2 cells were seeded in 96-well microplates at 5×10^4 cells per well for measurement of $[Ca^{2+}]_i$, 24-well plates at 2×10^4 cells per well for conditioned media collection and in 6-well plates at 1.5×10^5 cells per well for RNA extraction, and incubated overnight. The next day, cells were maintained in Opti-MEM™ Reduced Serum Medium (Gibco) and transfected with 50 nM Piezo1-specific siRNA (s107968, Thermo Fisher Scientific; siPiezo1) or negative control siRNA (4390843, Thermo Fisher Scientific; siCTL) using Lipofectamine™ RNAiMAX Transfection Reagent (Invitrogen) according to manufacturer's instructions. Twenty-four hours post transfection cells were used for indicated experiments. RT-qPCR was performed as described above to examine the Piezo1 mRNA expression level in transfected cells. The mRNA expression in cells trans-fected with siPiezo1 relative to that in cells transfected with siCTL was calculated using the $2^{-\Delta\Delta Ct}$ method (Livak & Schmittgen, 2001), where $\Delta\Delta C_t = [(Ct_{Piezo1} - Ct_{U6})_{siPiezo1} - (Ct_{Piezo1} - Ct_{U6})_{siCTL}]$.

2.8 | ELISA

Cells were plated in 24-well plates at 5×10^4 BV2 cells in 400 μl cul-ture media per well or in 96-well plates at 3.5×10^4 primary microglial cells in 200 μl culture media per well, and incubated for 24 h before use. Cells were treated with 100–1000 ng/ml LPS, 0.3–3 μM Yoda1 and/or 3 mM ATP for 2–24 h, as indicated, before the media was col-lected for ELISA analysis. For experiments, testing the effect of an antagonist or inhibitor, the compound at indicated concentrations was applied to cells 30 min before, and during, subsequent treatment with LPS or LPS and Yoda1. Media were centrifuged to remove cellular debris. The concentrations of pro-inflammatory cytokines in the condi-tioned culture media were measured using murine TNF-α, IL-1β, and IL-6 ABTS ELISA development kits (PeproTech) as per manufacturer's guidelines. In brief, 96-well plates were incubated with capture anti-bodies diluted in PBS overnight at room temperature before being washed with PBS containing 0.05% Tween-20. Plates were incubated in blocking buffer (1% bovine serum albumin [BSA] in PBS) for 1 h before addition of cytokine protein standards and media samples in triplicate and incubation for 2 h. Detection antibodies, diluted in PBS containing 0.05% Tween-20 and 0.1% BSA, were added and incubated for 2 h. An avidin-HRP conjugate solution was added for 30 min, fol-lowed by addition of the ABTS liquid substrate. The color change was detected by measuring absorbance at 405 nm using a Varioskan Flash Microplate Reader (Thermo Fisher Scientific), with background correc-tion measured at 650 nm. The concentration of cytokines in each media sample was derived from the standard curves.

2.9 | PI staining

Cell death was examined using a propidium iodide (PI) staining assay. Cells were exposed to treatments for 24 h and then incubated for 30 min at 37°C with PI and Hoechst 33342, both at a concentration
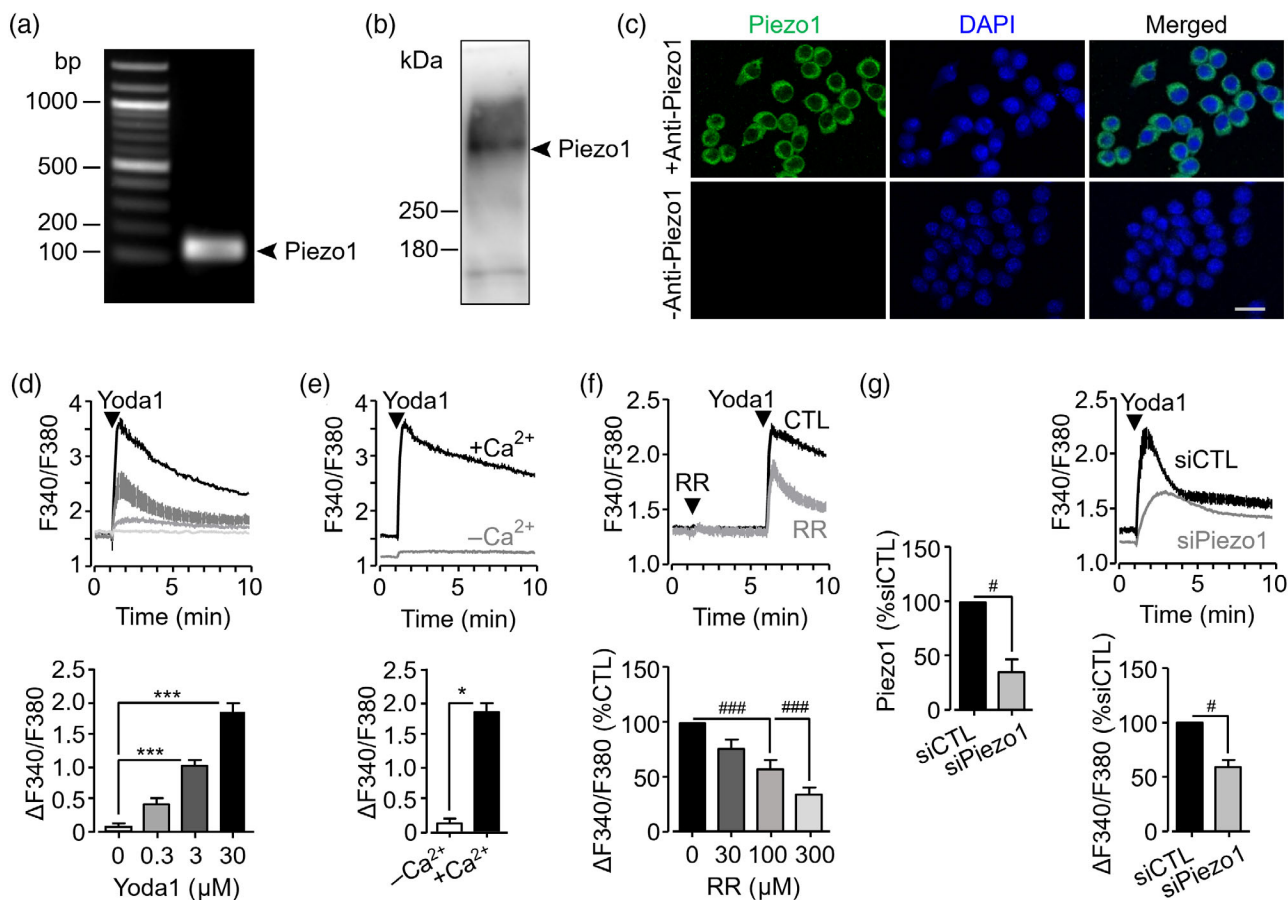
FIGURE 1 Characterization of Piezo1 expression and Yoda1-induced intracellular Ca^{2+} responses in BV2 microglial cells. (a) Agarose gel electrophoresis image showing the PCR product of Piezo1 with anticipated size. (b) Representative Western blot showing Piezo1 protein expression. (c) Representative immunofluorescent images demonstrating Piezo1 protein expression in cells stained with an anti-Piezo1 antibody or with secondary antibody alone, counterstained with DAPI. Scale bar is 25 μm. (d,e) Summary of intracellular Ca^{2+} responses to Yoda1 in extracellular Ca^{2+}-containing and Ca^{2+}-free solutions. Top: Representative recordings showing mean ± standard error of the mean (SEM) Ca^{2+} responses to indicated concentrations of 0, 0.3, 3 and 30 μM Yoda1 from 3 wells of cells in one experiment. Bottom: Mean ± SEM of mean peak Ca^{2+} responses from 3 repeats. Yoda1 (30 μM) was used in (e). (f) Summary of effect of treatment with ruthenium red (RR) on Ca^{2+} response to 10 μM Yoda1. Top: Representative recordings showing mean ± SEM Ca^{2+} response from 3 wells of cells in one experiment in control cells (CTL) or cells treated with 300 μM RR. Bottom: Mean ± SEM of mean peak Ca^{2+} responses from 4 repeats. (g) Summary of effect of siRNA transfection on Piezo1 expression examined by RT-qPCR. Left: Mean ± SEM Piezo1 expression in cells transfected with Piezo1-specific siRNA (siPiezo1), presented as % of that in cells transfected with control siRNA (siCTL), from three repeats. Right top: Representative recordings showing mean ± SEM Ca^{2+} responses from four wells of cells in one experiment to 10 μM Yoda1 in cells transfected with siPiezo1 and siCTL. Right bottom: Mean ± SEM of mean peak Ca^{2+} responses from 3 repeats. *$p < .05$; ***$p < .005$, compared to control conditions (d, e). #, $p < .05$; ###, $p < .005$, compared to treatment with Yoda1 (f) or transfection with siPiezo1 (g).

of 5 μg/ml. Fluorescent images were captured using an EVOS FL Auto Imaging System (Life Technologies). Cells stained by PI and Hoechst 33342 were analyzed using ImageJ, and cell death is presented by PI-positive cells as a percentage of all cells in the same image identified by counter-staining with Hoechst 33342.

2.10 | Characterization of cell morphology

Primary microglial cells were seeded in 96-well microplates at 2×10^4 cells per well and incubated overnight prior to treatment for 24 h with 100 ng/ml LPS and/or 3 μM Yoda1. Cells were imaged using an EVOS FL Auto Imaging System (Life Technologies) and cell morphology analyzed using ImageJ. The form factor of a cell was derived using the formula $4\pi \times area/perimeter^2$, with a value of 1 representing a circular shape and values closer to 0 an elongated shape (Soltys et al., 2001). The length-to-width ratio of the cell was termed the aspect ratio, with values closer to 1 indicating a more circular form (Zanier et al., 2015).

2.11 | Data presentation and statistical analysis

Data are presented as mean ± standard error of the mean (SEM), unless otherwise stated. The Shapiro–Wilk Normality test was used

to determine the data distribution. For comparisons of three or more groups, one-way ANOVA was performed to calculate statistical significance and Tukey's test for post hoc analysis of differences. For comparisons of two groups, Student's t-test was used. Statistical significance was accepted for values of $p < .05$. Statistical analysis was performed with SPSS Statistics software (version 27).

3 | RESULTS

3.1 | Piezo1 channel expression and its critical role in Yoda1-induced Ca^{2+} influx in BV2 microglial cells

We firstly examined the Piezo1 channel expression in BV2 cells, a widely used microglial cell line. Piezo1 expression at the mRNA and protein levels was detected by RT-qPCR (Figure 1a) and Western blotting (Figure 1b), respectively. Piezo1 protein expression in BV2 cells was also observed using immunofluorescence confocal imaging. Cells showed strong staining with the anti-Piezo1 antibody, which was absent in cells labeled with only the secondary antibody (Figure 1c). These results are overall consistent with a recent study reporting Piezo1 protein expression in BV2 cells (Liu et al., 2021).

The Piezo1 channel is a Ca^{2+}-permeable channel (Coste et al., 2010). We next examined the functional expression of the Piezo1 channel, using Fura-2, a ratiometric Ca^{2+} fluorescent indicator, in combination with a Flexstation microplate reader to measure intracellular Ca^{2+} response to application of Yoda1. In extracellular Ca^{2+}-containing solutions, application of 0.3, 3 and 30 μM Yoda1 induced a robust and concentration-dependent increase in [Ca^{2+}]$_i$, with the increase reaching a significant level at 3 μM (Figure 1d). In contrast, application of Yoda1 even at 30 μM elicited little or no Ca^{2+} response in extracellular Ca^{2+}-free solution (Figure 1e), which clearly indicates that the Piezo1 channel functions on the cell surface and mediates Ca^{2+} influx to raise the [Ca^{2+}]$_i$. Treatment with 30, 100, and 300 μM RR, a compound known to inhibit the Piezo1 channel (Coste et al., 2010), prior to and during application of Yoda1, resulted in a concentration-dependent reduction of Yoda1-induced increase in [Ca^{2+}]$_i$ (Figure 1f). Compared to transfection with siCTL, transfection with siPiezo1 resulted in a significant reduction in the Piezo1 expression level and, consistently, Yoda1-induced increase in [Ca^{2+}]$_i$ (Figure 1g).

Taken together, these results provide clear evidence to show that the Piezo1 channel is expressed at the cell surface as a Ca^{2+}-permeable channel in BV2 microglial cells.

3.2 | Piezo1 channel activation inhibits LPS-induced microglial cell activation and pro-inflammatory mediator production in BV2 microglial cells

We were interested in the role of the Piezo1 channel in regulating microglial cell activation and the pro-inflammatory phenotype by examining production of IL-1β, TNF-α and IL-6 in LPS-primed BV2 cells using ELISA. Priming with 100 ng/ml LPS strongly stimulated the production of both TNF-α and IL-6 (Figure 2a). Priming with LPS at 100 ng/ml or higher concentrations (300 and 1000 ng/ml) resulted in no significant increase in IL-1β production (Figure S1a). Interestingly, application of 0.3–3 μM Yoda1 during LPS priming led to a concentration-dependent reduction in the production of TNF-α and IL-6 (Figure 2b), without affecting IL-1β production (Figure S1b). The reduction in LPS-induced production of TNF-α and IL-6 reached statistical significance at the concentration of 1 and 3 μM Yoda1, respectively (Figure 2b). Application of Yoda1 to BV2 cells without LPS priming did not alter the low basal production of IL-1β, TNF-α, and IL-6 (Figure S1c). To better understand the inhibitory effect of Yoda1, we further analyzed the production of TNF-α and IL-6 in BV2 cells following exposure to 100 ng/mL LPS and 3 μM Yoda1 for different durations (2, 4, 8, 12, 24 h). LPS-induced production of TNF-α and IL-6 peaked at 8 h and, importantly, was significantly reduced by treatment with Yoda1 by this point (Figure 2c). Exposure to 100 ng/ml LPS, 3 μM Yoda1 or in combination for 24 h did not induce cell death assessed using PI staining (Figure S2), excluding the possibility that necrotic cell death causes cytolytic release of TNF-α and IL-6 into the culture medium. Collectively, these results reveal a critical role of the Piezo1 channel in downregulating the pro-inflammatory response, particularly inhibiting the production of TNF-α and IL-6 by BV2 microglial cells.

More effective IL-1β production or, more specifically, its efficient processing and secretion requires a second signal that activates the NLRP3 inflammasome and subsequently caspase-1 to convert pro-IL-1β to IL-1β. A high concentration of extracellular ATP, often associated with tissue inflammation and damage, is well known as an activation signal through the P2X7 receptor to promote NLRP3 inflammasome activation and IL-1β production (Pelegrin, 2021). Treatment of BV2 cells with 100–1000 ng/ml LPS and 3 mM ATP increased the production of IL-1β (cf. Figures S1a and S3a). Under such conditions, treatment with Yoda1 still significantly but less effectively inhibited TNF-α production and resulted in slight but insignificant increase in the production of IL-1β and IL-6 (Figure S3b). Overall, these results are consistent with the well-established role of the P2X7 receptor in stimulating production of pro-inflammatory cytokines including TNF-α and IL-6, which mitigates the inhibition imposed by Piezo1 channel activation. Interestingly, recent studies by us and others examining different cell types provide strong evidence to support ATP release and activation of P2 receptors as a common and important mechanism transducing Piezo1 channel activation to regulation of cell function (Wei et al., 2019). We were interested in the role of such a signal transduction mechanism in Yoda1-induced Piezo1 channel-mediated inhibition of the production of TNF-α and IL-6 in microglial cells. Treatment with 3 units/ml apyrase, an enzyme that catalyzes the hydrolysis of ATP, prior to and during exposure to LPS and Yoda1, significantly reduced Yoda1-induced inhibition of TNF-α production, and almost abolished Yoda1-induced inhibition of IL-6 production (Figure S4a), without effect on LPS-induced production of TNF-α
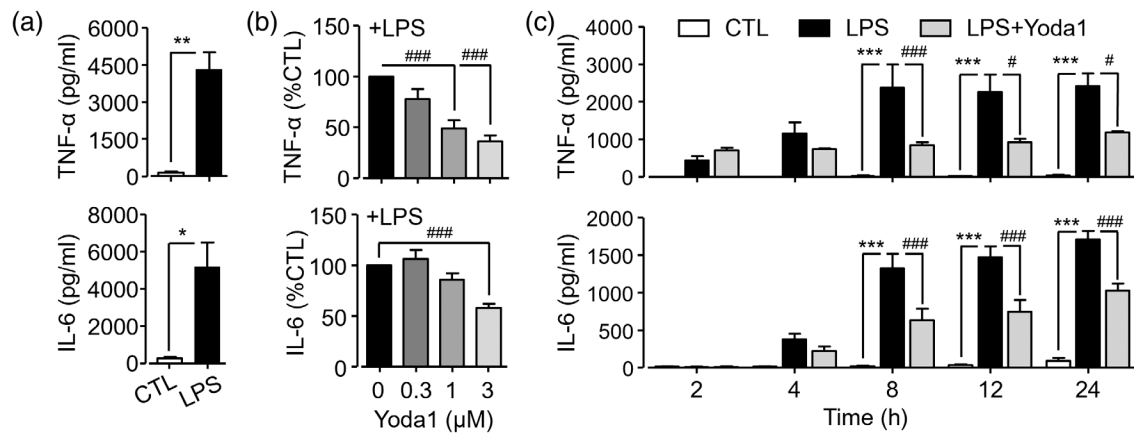
FIGURE 2 Piezo1 channel activation inhibits lipopolysaccaharide (LPS)-induced generation of pro-inflammatory cytokines from BV2 microglial cells. (a) Summary of tumor necrosis factor (TNF)-α (top) and IL-6 (bottom) released from control cells and cells primed with 100 ng/ml LPS for 24 h. (b) Summary of TNF-α (top) and IL-6 (bottom) released from LPS-primed BV2 cells without or with exposure to the indicated concentrations of Yoda1 for 24 h. (c) Summary of TNF-α (top) and IL-6 (bottom) released from control cells, cells primed with LPS, and cells primed with LPS with and treated with 3 μM Yoda1 for 2, 4, 8, 12 and 24 h. Data are displayed as mean ± SEM concentration (a, c) or % of that in cells primed with LPS (b), from 3 (c top), 4 (a top, b bottom, c bottom), or 5 (a bottom, b top) repeats. *$p < .05$; **$p < .01$; ***$p < .005$ compared to control conditions. #, $p < .05$; ###, $p < .005$ compared to priming with LPS.

and IL-6 (Figure S4b), suggesting that ATP is released as a result of Piezo1 channel activation. Treatment with 30 μM PPADS, a generic P2 receptor antagonist, prior to and during exposure to LPS and Yoda1, however, did not affect the production of TNF-α and IL-6 (Figure S4c). Such treatment also had no effect on LPS-induced production of TNF-α and IL-6 (Figure S4d). PPADS is known to display poor sensitivity in inhibiting the P2X7 receptor (North & Surprenant, 2000). Treatment with 1 μM AZ11645373 or A740003, two P2X7-specific and structurally different antagonists, prior to and during exposure to LPS and Yoda1, induced a tiny, albeit statistically significant, reduction in Yoda1-induced inhibition of TNF-α production (Figure S4e), without effect on LPS-induced TNF-α production (Figure S4f). In summary, these results suggest that ATP release is at least part of the mechanism transducing Piezo1 channel activation to inhibition of the pro-inflammatory function of microglial cells with a minimal role for the P2 receptors including the P2X7 receptor.

3.3 | Piezo1 channel-mediated Ca^{2+} signaling is important for inhibition of LPS-induced NF-κB activation in BV2 microglial cells

As introduced above, intracellular Ca^{2+} signaling is important in regulating gene expression, and NF-κB is one of the major transcription factors that is activated as part of the Ca^{2+}-dependent downstream signaling pathways to drive the expression of cytokines by activated microglial cells (Dresselhaus & Meffert, 2019). Mechanistically, it has been well established that NF-κB activation is accompanied by its translocation from the cytosol to the nucleus. Therefore, we examined the effects of treatment with Yoda1 on the activation of this pathway in LPS-primed BV2

cells. LPS priming resulted in a strong increase in the proportion of NF-κB in the nucleus, revealed by immunofluorescence confocal imaging (Figure 3a,b), indicating that LPS priming promotes activation of the NF-κB pathway. Such nuclear translocation was almost completely prevented by treatment with Yoda1 (Figure 3a,b).

To gain mechanistic insights into Piezo1 channel-mediated inhibition of LPS-induced NF-κB activation, we next determined the phosphorylation of p65 protein, a key event in the activation of the multiple-protein NF-κB signaling complex, as well as its total protein expression level using Western blotting. LPS priming for 24 h strongly increased p65 phosphorylation without altering its protein expression level, and treatment with Yoda1 during LPS priming suppressed p65 phosphorylation but not protein expression (Figure 3c,d). Such an inhibition was also detected in cells after treatment with LPS and Yoda1 for 6 h (Figure S5). These results clearly indicate that Piezo1 channel activation inhibits LPS-induced NF-κB activation. Furthermore, we examined the role of Piezo1 channel-mediated Ca^{2+} signaling in Yoda1-induced inhibition of NF-κB activation in LPS-primed BV2 cells. Treatment with 1 μM BAPTA-AM, an intracellular Ca^{2+} chelator, prior to and during exposure to LPS and Yoda1, largely abolished Yoda1-induced inhibition of NF-κB nuclear translocation, as shown using immunofluorescence confocal imaging (Figure 3e,f). Taken together, these results support that Piezo1 channel-mediated Ca^{2+} signaling is important for inhibition of LPS-induced activation of the NF-κB pathway in BV2 microglial cells.

To further validate the role of the Piezo1 channel in mediating Yoda1-induced inhibition of the pro-inflammatory response in microglial cells, we compared NF-κB activation and TNF-α production in BV2 cells transfected with siCTL and siPiezo1 prior to treatment with LPS and Yoda1 for 24 h. As shown above in
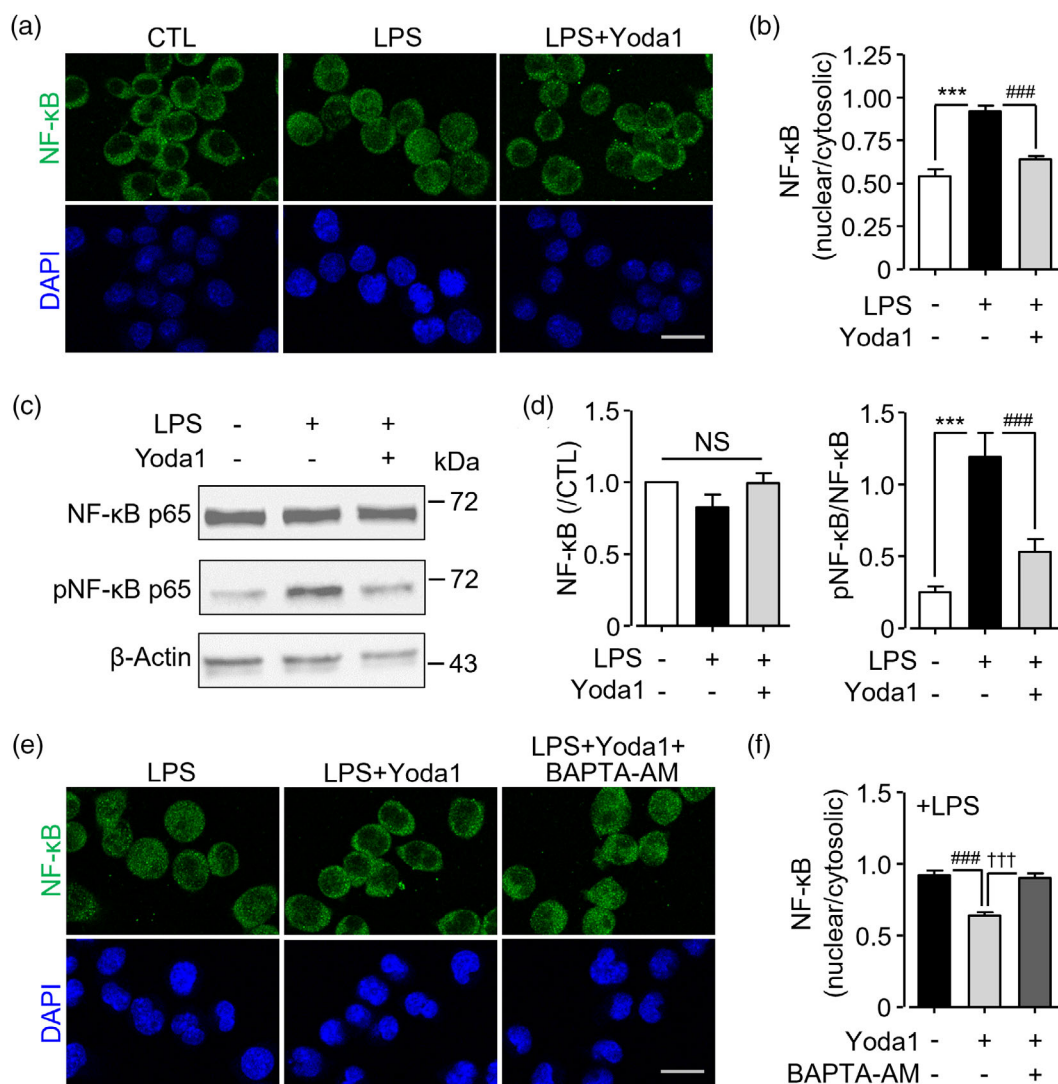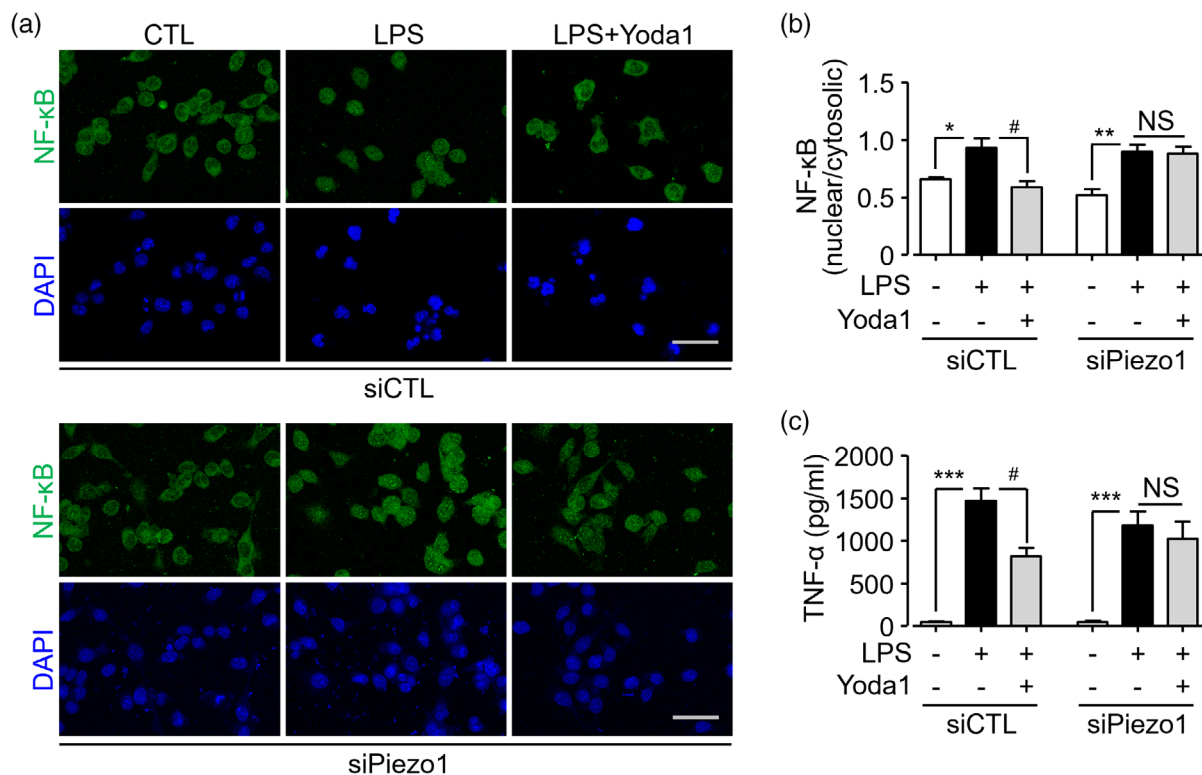
FIGURE 3 Piezo1 channel activation inhibits lipopolysaccharide (LPS)-induced activation and nuclear translocation of NF-κB in BV2 microglial cells. (a) Representative immunofluorescent confocal images showing subcellular location of NF-κB p65 protein in control cells, cells primed with 100 ng/ml LPS and cells primed with LPS and treated with 3 μM Yoda1 for 24 h. Cells were counterstained with DAPI. (b) Summary of the mean ratio of nuclear and cytosolic p65 in cells as shown in (a). (c) Representative Western blots showing protein expression and the phosphorylated form of the p65 subunit of NF-κB in control cells and cells primed with 100 ng/ml LPS without or with treatment with 3 μM Yoda1 for 24 h. (d) Summary of the total expression of p65 and the ratio of total p65 to phosphorylated p65 in cells as shown in (c). (e) Representative immunofluorescent confocal images showing subcellular location of NF-κB p65 protein in cells primed with 100 ng/ml LPS without or with treatment with 3 μM Yoda1, and in cells treated with 1 μM BAPTA-AM for 1 h prior to and during exposure to LPS and Yoda1. Cells were counterstained with DAPI. (f) Summary of the mean ratio of nuclear and cytosolic p65 in cells as shown (e). Scale bars are 20 μm. Data are displayed as mean ± standard error of the mean (SEM) from 4 (b) or 5 (d,f) repeats. ***$p < .005$ compared to control conditions. ###, $p < .005$ compared to priming with LPS. †††, $p < .005$ compared to priming with LPS and treatment with Yoda1. NS, not significant.

nontransfected cells, application of 3 μM Yoda1 still strongly inhibited NF-κB nuclear translocation and, in strong contrast, such Yoda1-induced inhibition of NF-κB activation was largely blunted in cells transfected with siPiezo1 (Figure 4a,b). Consistently, application of Yoda1 strongly inhibited LPS-induced TNF-α production in siCTL-transfected cells, but not in siPiezo1-transfected cells (Figure 4c). Collectively, these results provide further evidence to support the notion that Piezo1 channel activation inhibits the LPS-induced pro-inflammatory response via inhibiting the NF-κB inflammatory signaling pathway.

3.4 | Expression of the Piezo1 channel with an important role in mediating Yoda1-induced Ca²⁺ signaling in primary mouse microglial cells

BV2 cells, as demonstrated in this and many previous studies, can be useful in elucidating molecular and signaling mechanisms regulating microglial cell functions. However, increasing evidence indicates BV2 cells can differ from primary microglial cells functionally, as well as morphologically (Das et al., 2016; He et al., 2018; Luan et al., 2022). Therefore, we performed experiments using primary microglial cells isolated from mice to validate

FIGURE 4 Piezo1 knockdown attenuates Yoda1-mediated inhibition of lipopolysaccharide (LPS)-induced NF-κB activation and tumor necrosis factor (TNF)-α production in BV2 microglial cells. (a) Representative immunofluorescent confocal images showing subcellular location of NF-κB p65 protein in cells transfected with control siRNA (siCTL) or Piezo1-specific siRNA (siPiezo1) under control conditions or primed with 100 ng/ml LPS in the presence and absence of 3 μM Yoda1 for 24 h. Cells were counterstained with DAPI. Scale bars are 50 μm. (b) Summary of the mean ratio of nuclear and cytosolic p65 in cells transfected with siCTL or siPiezo1 as shown in (a). (c) Summary of TNF-α released from BV2 cells transfected with siCTL or siPiezo1 prior to exposure to LPS, or LPS with Yoda1 for 24 h. Data are displayed as mean ± standard error of the mean (SEM) from 3 (b) or 4 (c) repeats. *$p < .05$; **$p < .01$; ***$p < .005$ compared to control conditions. #, $p < .05$ compared to priming with LPS. NS, not significant.

the key findings from BV2 cells described above. The Piezo1 mRNA expression in primary microglial cells was demonstrated using RT-qPCR (Figure 5a), and the protein expression using Western blotting and immunofluorescence confocal imaging (Figure 5b,c), respectively. Consistently, application of 1, 3, 10, and 30 μM Yoda1 to primary microglial cells in extracellular Ca^{2+}-containing solution induced a concentration-dependent increase in $[Ca^{2+}]_i$ (Figure 5d). Such Ca^{2+} response was almost completely absent in extracellular Ca^{2+}-free solution (Figure 5e). Furthermore, treatment with 30, 100 and 300 μM RR also led to a concentration-dependent reduction in Yoda1-induced Ca^{2+} responses (Figure 5f). These results show that the Piezo1 channel functions on the cell surface as a Ca^{2+}-permeable channel and mediates Yoda1-induced Ca^{2+} influx to increase $[Ca^{2+}]_i$ in primary mouse microglial cells, as shown above in BV2 cells.
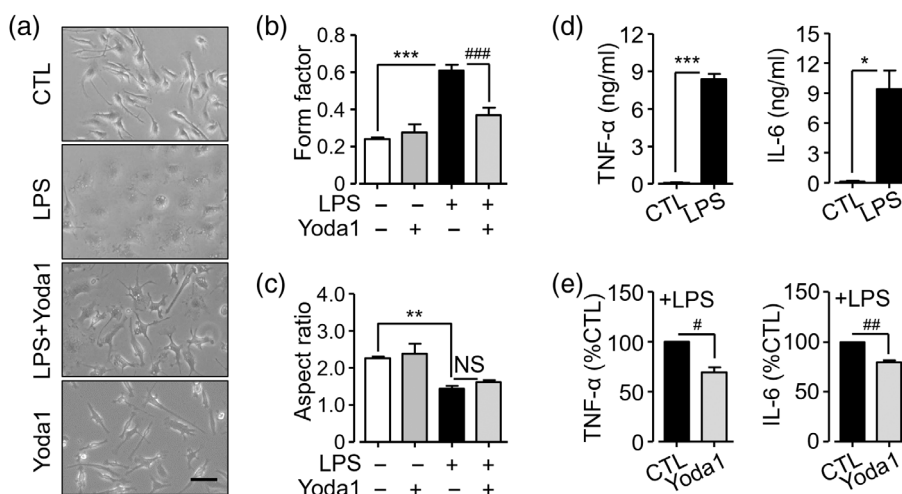
3.5 | Piezo1 channel activation inhibits LPS-induced microglial cell activation and pro-inflammatory mediator generation in primary mouse microglial cells

Differing from BV2 cells, primary microglial cells under in vitro culture conditions, as observed in vivo, for example, in the brain (Boche

et al., 2019), exhibit a dynamic range of morphologies, which are associated with their functional states. Mouse microglial cells under resting condition, that is, without LPS priming, displayed the well-documented cell morphology with elongated processes stemming from the cell body (Figure 6a). After priming with 100 ng/ml LPS for 24 h, they underwent a striking morphological change, and adopted an amoeboid shape and occupied a noticeably larger area (Figure 6a), indicating microglial cell activation. Such morphological change was quantitatively characterized by analysis of individual cells that showed a significant increase in the form factor and a decrease in the aspect ratio (Figure 6b,c). LPS-induced morphological change was strongly attenuated by treatment with 3 μM Yoda1 during LPS priming (Figure 6a,b). LPS priming of primary microglial cells resulted in a dramatic increase in the production of TNF-α and IL-6 (Figure 6d), without significant effect on IL-1β production (Figure S6a). Importantly, as shown above with BV2 cells, treatment of primary microglial cells with 3 μM Yoda1 during LPS priming significantly reduced the production of TNF-α and IL-6 (Figure 6e), causing no significant effect on IL-1β production in LPS-primed cells (Figure S6b). In primary microglial cells without LPS priming, treatment with Yoda1 had no effect on cell morphology (Figure 6a–c) or production of TNF-α and IL-6, though it did induce a modest reduction in IL-1β production (Figure S6c). We also
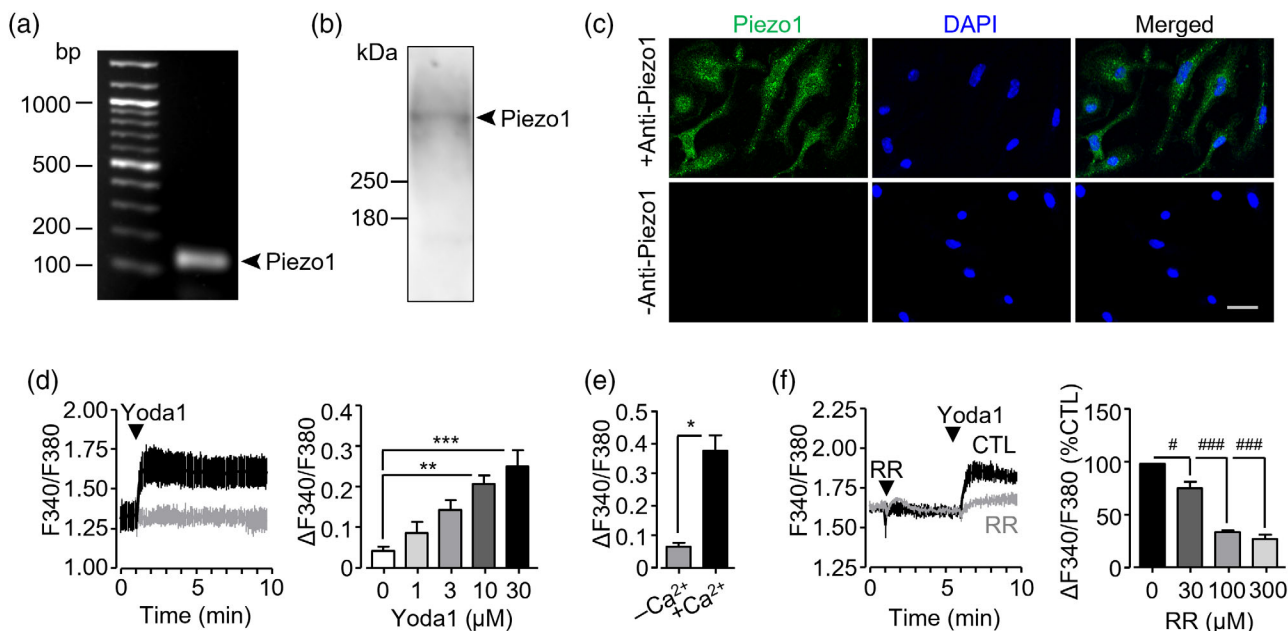
FIGURE 5 Characterization of Piezo1 expression and Yoda1-induced intracellular Ca^{2+} responses in primary mouse microglial cells. (a) Representative agarose gel electrophoresis image showing the PCR product of Piezo1 with anticipated size. (b) Representative Western blot showing Piezo1 protein expression. (c) Representative immunofluorescent images demonstrating Piezo1 protein expression in cells stained with an anti-Piezo1 antibody or secondary antibody alone. Cells were counterstained with DAPI. Scale bar is 25 μm. (d) Summary of intracellular Ca^{2+} responses to Yoda1 in extracellular Ca^{2+}-containing solutions. Left: Representative recordings showing mean ± standard error of the mean (SEM) Ca^{2+} responses to 30 μM Yoda1 from 3 wells of cells in one experiment. Right: Mean ± SEM of mean peak Ca^{2+} responses from 3 repeats. (e) Summary of mean peak intracellular Ca^{2+} responses to 10 μM Yoda1 in extracellular Ca^{2+}-containing and Ca^{2+}-free solutions, from 3 repeats. (f) Summary of effect of treatment with ruthenium red (RR) on Yoda1-induced Ca^{2+} responses. Left: Representative recordings showing mean ± SEM Ca^{2+} responses from 3 wells of cells in one experiment under control conditions or treatment of cells with RR for 5 min prior to exposure to 10 μM Yoda1. Right: Mean ± SEM of mean peak Ca^{2+} responses from 3 repeats. $*p < .05$; $**p < .01$; $***p < .005$ compared to control conditions. #, $p < .05$; ###, $p < .005$, compared to treatment with Yoda1.

FIGURE 6 Piezo1 channel activation inhibits lipopolysaccharide (LPS)-induced microglial cell activation and pro-inflammatory mediator production in primary mouse microglial cells. (a) Representative phase contrast microscopic images showing morphology of control (CTL) cells, cells primed with 100 ng/ml LPS without or with treatment with 3 μM Yoda1, and cells treated with Yoda1 alone for 24 h. Scale bar is 50 μm. (b, c) Characterization of form factor (b) and aspect ratio (c) of cells as shown in (a). Data are displayed as mean ± SEM from 450 cells from 3 repeats, with 150 cells analyzed in each repeat. (d) Summary of tumor necrosis factor (TNF)-α (left) and IL-6 (right) released from control cells and cells primed with 100 ng/ml LPS for 24 h. Data are displayed as mean ± SEM from 3 repeats. (e) Summary of TNF-α (left) and IL-6 (right) released from LPS-primed cells without (CTL) or with treatment with 3 μM Yoda1 for 24 h. Data are displayed as mean ± SEM from 3 repeats. $*p < .05$; $**p < .01$; $***p < .005$, compared to control conditions. #, $p < .05$; ##, $p < .01$; ###, $p < .005$ compared to priming with LPS. NS, not significant.
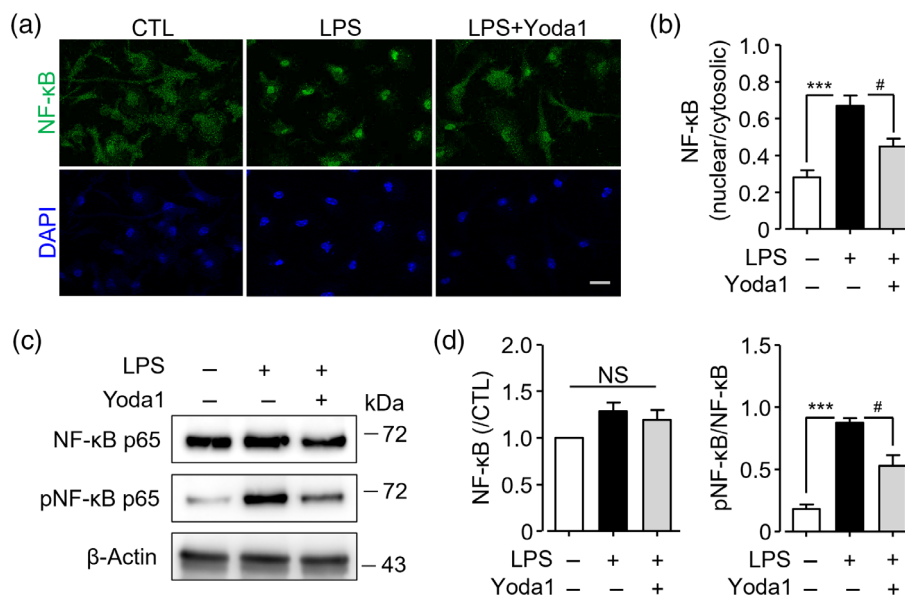
FIGURE 7 Piezo1 channel activation inhibits lipopolysaccharide (LPS)-induced activation and nuclear translocation of NF-κB in primary microglial cells. (a) Representative immunofluorescent confocal images showing subcellular location of NF-κB p65 protein in control cells and cells primed with 100 ng/ml LPS in the presence and absence of 3 μM Yoda1 for 24 h. Cells were counterstained with DAPI. Scale bar is 20 μm. (b) Summary of the mean ratio of nuclear and cytosolic p65 in cells as shown in (a). (c) Representative Western blots showing protein expression and the phosphorylated form of the p65 subunit of NF-κB in control cells and cells primed with 100 ng/ml LPS without or with treatment with 3 μM Yoda1 for 24 h. (d) Summary of total expression of p65 and the ratio of total p65 to phosphorylated p65 in cells as shown in (c). Data are displayed as mean ± SEM from 3 (d) or 4 (b) repeats. ***$p < .005$ compared to control conditions. #, $p < .05$; compared to priming with LPS. NS, not significant.

examined primary mouse microglial cells treated with 100 ng/ml LPS and 3 mM ATP; application of Yoda1 resulted in no inhibition of the production of TNF-α, IL-6 and IL-1β (Figure S6d). Therefore, these results from primary mouse microglial cells are overall in strong agreement with the results from BV2 cells, albeit bearing some minor variations, and overall provide further supporting evidence that Piezo1 channel activation inhibits microglial cell activation and proinflammatory response.

3.6 | Piezo1 channel activation inhibits LPS-induced NF-κB activation in primary mouse microglial cells

We next investigated whether Piezo1 channel activation inhibits LPS-induced microglial cell activation and pro-inflammatory mediator production in primary mouse microglial cells also via suppression of the NF-κB inflammatory signaling pathway. LPS priming resulted in a strong increase in the proportion of NF-κB in the nucleus, indicating nuclear translocation and activation of NF-κB (Figure 7a,b). Such nuclear translocation was significantly reduced by application of 3 μM Yoda1 during LPS priming (Figure 7a,b). Furthermore, concurrent with NF-κB activation, LPS priming significantly increased the phosphorylation level of p65 protein, without affecting its total protein expression level after treatment for 24 h, and LPS-induced phosphorylation of p65 was notably reduced by treatment with Yoda1 (Figure 7c,d). In

primary mouse microglial cells, such inhibition of NF-κB activation by Piezo1 channel activation was also observed as early as 6 h after exposure to LPS and Yoda1 (Figure S7). These results from primary mouse microglial cells are highly consistent with the results from BV2 cells, and together provide strong evidence to indicate that Piezo1 channel activation reduces microglial cell activation and production of TNF-α and IL-6 by inhibiting the NF-κB signaling pathway.

3.7 | Activation of ERK1/2 and p38, which is critical for LPS-induced production of TNF-α and IL-6, is not targeted for inhibition by the Piezo1 channel

Extracellular signal-regulated kinase (ERK1/2) and p38 mitogen-activated protein kinases (MAPKs) have been linked to regulation of the NF-κB signaling pathway in microglial cells and other cell types (Moon et al., 2007; Plotnikov et al., 2011; Santa-Cecília et al., 2016). Therefore, we were interested in the role of ERK1/2 and p38 in mediating LPS-induced production of TNF-α and IL-6 and, in particular, the inhibitory effect of Piezo1 channel activation. LPS priming stimulated activation of ERK1/2, indicated by protein phosphorylation revealed by Western blotting, in both BV2 cells (Figure S8a) and primary mouse microglial cells (Figure S8b). Treatment of BV2 cells with 1 μM U0126, an inhibitor of MEK1/2 responsible for phosphorylation and thereby activation of ERK1/2, prior to and during LPS priming, resulted in a significant reduction in LPS-induced production of TNF-α and IL-6
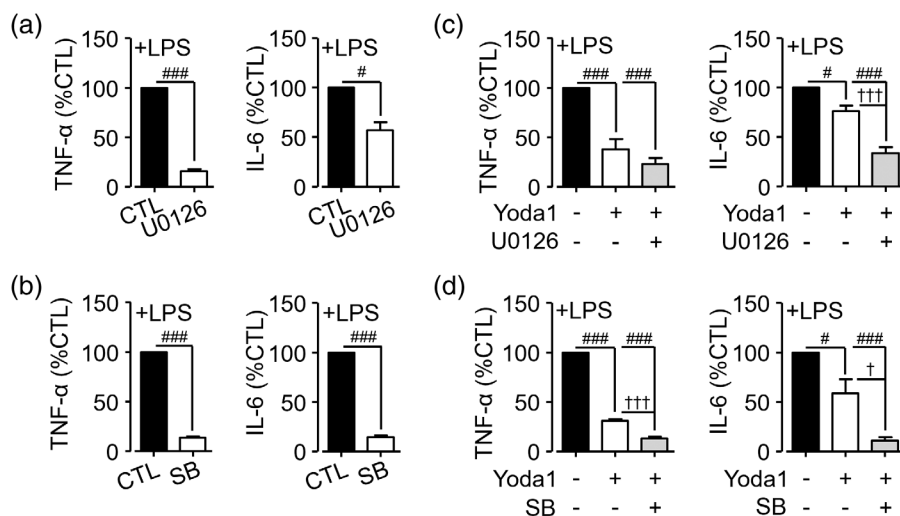
FIGURE 8 Lipopolysaccharide (LPS) stimulates ERK1/2 and p38 signaling to induce pro-inflammatory mediator production in BV2 microglial cells. (a, b) Summary of tumor necrosis factor (TNF)-α (left) and IL-6 (right) released from cells primed with 100 ng/ml LPS after 24 h, without or with pre-treatment with 1 μM U0126 (a) or 3 μM SB203580 (SB) (b). (c, d) Summary of TNF-α (left) and IL-6 (right) released from LPS-primed cells in the absence or presence of Yoda1 (3 μM) without or with pre-treatment with 1 μM U0126 (c) or 3 μM SB203580 (d), for 24 h. Data are displayed as mean ± standard error of the mean (SEM) as % of that in cells primed with LPS alone from 3 repeats. #, $p < .05$; ###, $p < .005$ compared to priming with LPS. †, $p < .05$; †††, $p < .005$, compared to priming with LPS and treatment with Yoda1.

(Figure 8a). LPS priming also stimulated p38 activation in primary mouse microglial cells (Figure S8b) and to a lesser extent in BV2 cells (Figure S8a). Treatment of BV2 cells with 3 μM SB203580, an inhibitor of p38, significantly reduced LPS-induced production of TNF-α and IL-6 (Figure 8b). Taken together, these results support the notion that activation of ERK1/2 and p38 is critical for LPS-induced production of TNF-α and IL-6. Treatment of LPS-primed cells with 3 μM Yoda1 resulted in slight but insignificant change in the activation level of both ERK1/2 and p38 in BV2 cells (Figure S8c) and primary microglial cells (Figure S8d). Co-treatment of BV2 cells with U0126 or SB203580 and Yoda1 reduced LPS-induced production of TNF-α and IL-6, to a similar or greater extent relative to each treatment alone (Figure 8c,d). Collectively, these results indicate that neither ERK1/2 nor p38 is targeted for inhibition by the Piezo1 channel, although activation of ERK1/2 and p38 is critical for LPS-induced production of TNF-α and IL-6 in microglial cells (Figure 9).

4 | DISCUSSION

Microglial cells in the CNS have a dual role in supporting neuronal cell function and mediating neuroinflammation that contributes to various types of CNS damage and disease (Orihuela et al., 2016; Wolf et al., 2017). The functional phenotypes of microglial cells are vital to their physiological or pathological role, and therefore it is important to understand the intrinsic mechanisms for external signals that regulate microglial cell function. Here, we provide evidence to show the Ca²⁺-permeable Piezo1 channel expressed on the cell surface in microglial cells as a previously unrecognized mechanism that is important in regulating the pro-inflammatory phenotype of microglial cells (Figure 9).
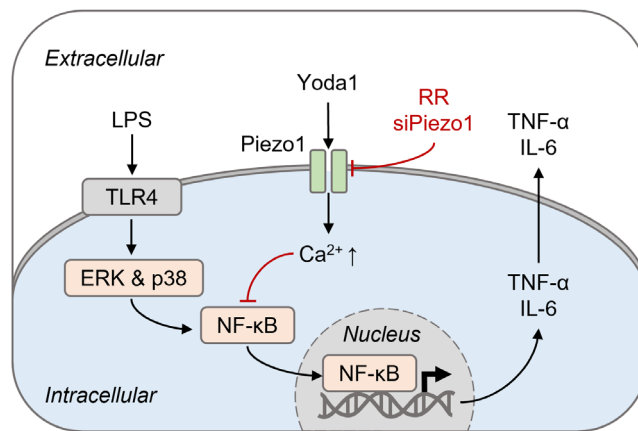
FIGURE 9 Piezo1 channel-mediated Ca²⁺ signaling inhibits lipopolysaccharide (LPS)-induced activation of the NF-κB inflammatory signaling pathway and generation of pro-inflammatory cytokines tumor necrosis factor (TNF)-α and IL-6 in microglial cells. Schematic summary of the key findings from this study. Priming with lipopolysaccharide (LPS) induces microglial cell activation via toll-like receptor 4 (TLR4), leading to ERK1/2 and p38-dependent activation of the NF-κB inflammatory signaling pathway to drive expression and production of TNF-α and IL-6. Piezo1 channel activation using Yoda1 results in an increase in intracellular Ca²⁺, which is inhibited by ruthenium red (RR) or depletion of Piezo1 expression using Piezo1-specific siRNA (siPiezo1). Piezo1 channel activation attenuates LPS-induced NF-κB activation and nuclear translocation and thereby the production of TNF-α and IL-6.

4.1 | Piezo1 is expressed as a Ca²⁺-permeable channel on the cell surface of microglial cells

Piezo1 expression in microglial cells has been demonstrated in BV2 cells by a recent study using Western blotting (Liu et al., 2021). Here,

we confirmed Piezo1 mRNA and protein expression in BV2 cells, using RT-qPCR, Western blotting and immunofluorescence confocal imaging (Figure 1a–c). We also demonstrated Piezo1 mRNA and protein expression in primary mouse microglial cells (Figure 5a–c). Importantly, we showed in both BV2 cells and primary microglial cells that exposure to Yoda1 induced robust increases in $[Ca^{2+}]_i$ that almost entirely resulted from extracellular Ca^{2+} influx (Figures 1d,e and 5d,e). Furthermore, Yoda1-induced Ca^{2+} responses in both BV2 cells and primary microglial cells were significantly attenuated by treatment with the Piezo1 inhibitor RR (Figures 1f and 5f). Yoda1-induced increase in $[Ca^{2+}]_i$ in BV2 cells was also significantly reduced by siRNA-mediated knockdown of Piezo1 expression (Figure 1g). Taken together, these results from pharmacological and genetic interventions provide the first functional evidence that consistently supports that Piezo1 is expressed in microglial cells as a Ca^{2+}-permeable channel in the plasma membrane, as reported in various other cell types (Fang et al., 2021). It is anticipated, though further experiments are required to demonstrate, that Piezo1 channel activity in microglial cells can be induced by mechanical stimulation, as well as chemical stimulation.

4.2 | Piezo1 channel activation inhibits LPS-induced microglial cell activation and pro-inflammatory mediator production

An important finding of this study is that the Piezo1 channel in microglial cells plays a critical role in regulating pro-inflammatory phenotypes following LPS-induced activation in both BV2 cells and primary mouse microglial cells. There was far less noticeable morphological change in BV2 cells upon exposure to LPS. As documented by previous studies, primary microglial cells exhibited a dramatic change in cell morphology accompanying activation induced by LPS priming (Figure 6a–c). Such morphological change was strongly attenuated by Yoda1-induced Piezo1 channel activation (Figure 6a–c). In BV2 cells and primary microglial cells, exposure to 100 ng/ml LPS induced production of TNF-α and IL-6 (Figures 2a and 6d). However, such LPS priming resulted in no significant increase in IL-1β production in BV2 cells or primary microglial cells (Figure S1a and Figure S4a). Some previous studies reported that exposure to 500–1000 ng/ml LPS induced IL-1β production in microglial cells (Jeong et al., 2013; Moraes et al., 2015). As we tested here in BV2 cells, there was no increase in IL-1β production after priming with 300–1000 ng/ml LPS for 24 h (Figure S1a). Piezo1 channel activation in LPS-induced activated microglial cells strongly reduced the production of TNF-α and IL-6 (Figures 2b,c and 6e), without effect on IL-1β production (Figures S1b and S6b). These results were consistently observed in both BV2 cells and primary microglial cells. In microglial cells under resting conditions, namely without LPS priming, Piezo1 channel activation had little effect on the basal level of TNF-α and IL-6 produced by BV2 cells (Figure S1c) and primary microglial cells (Figure S6c), as well as no effect on morphology in primary microglial cells (Figure 6a–c). Piezo1 channel activation also did not affect IL-1β production in BV2 cells

(Figure S1b) but slightly decreased in IL-1β production in primary microglial cells (Figure S6c), which may be attributed to the functional difference between BV2 and primary microglial cells. Regardless, our results collectively indicate that Piezo1 channel activation inhibits LPS-induced microglial cell activation and production of TNF-α and IL-6. A recent study shows that Piezo1 channel activation, also induced chemically by application of Yoda1, reduced LPS-induced production of TNF-α and IL-6, and also IL-1β in astrocytes (Velasco-Estevez et al., 2020). While the reasons for differences in the effect on LPS-induced IL-1β production in microglial cells and astrocytes are unclear, these findings are consistent in supporting that Piezo1 channel activation in both microglial cells and astrocytes, the two major glial cells in the CNS, suppress their pro-inflammatory phenotypes, including the production of pro-inflammatory cytokines. A role for the Piezo1 channel in attenuating inflammation has also recently been described in adipocytes, with genetic reduction of Piezo1 expression increasing the mRNA expression of IL-1β, IL-6, and TNF-α in mice fed a high fat diet (Zhao et al., 2019a). Furthermore, TNF-α mRNA expression in primary adipocytes was reduced by Yoda1-induced Piezo1 channel activation and, conversely, increased following inhibition of the Piezo1 channel with GsMTx4 (Zhao et al., 2019a). However, it is worth pointing out that other recent studies have reported that Piezo1 channel activation stimulates pro-inflammatory responses in macrophages, myeloid cells and nucleus pulposus cells (Atcha et al., 2021; Solis et al., 2019; Sun et al., 2022). For example, Yoda1-induced Piezo1 channel activation in bone marrow-derived macrophages enhanced the pro-inflammatory response to exposure to a combination of LPS and interferon-γ (Atcha et al., 2021). Similarly, mechanical activation of the Piezo1 channel in nucleus pulposus cells resulted in NLRP3 inflammasome activation and IL-1β production (Sun et al., 2020). Therefore, the role of the Piezo1 channel in the regulation of an inflammatory response appears cell type-specific, which is intriguing and, as postulated in a recent study (Velasco-Estevez et al., 2020), may depend on the signaling mechanisms downstream of Piezo1 channel activation.

4.3 | ATP-induced purinergic signaling and Piezo1 channel activation in the regulation of LPS-induced production of pro-inflammatory cytokines

Recent studies have examined the role of the Piezo1 channel in many different cell types in regulating diverse processes, leading to the finding that ATP release and activation of P2 receptors is an important mechanism that transduces Piezo1 channel activation to regulation of cell functions (Wei et al., 2019). Such a signal transduction mechanism has been described in regulating red blood cell volume (Cinar et al., 2015), bladder function in urothelial cells (Miyamoto et al., 2014), vascular function in endothelial cells (Wang et al., 2016), surfactant secretion in alveolar cells (Diem et al., 2020), and migration of mesenchymal stem cells (Mousawi et al., 2020). More recently, studies have shown a critical role of ATP release in Piezo1 channel-mediated cholangiocyte (Desplat et al., 2021) and odontoblast

function (Sun et al., 2022). In this study, we showed using BV2 cells that inclusion of ATP-scavenging apyrase in the culture medium consistently increased the production of TNF-α and IL-6 in cells exposed to LPS and Yoda1 (Figure S4a), without effect on the production of TNF-α and IL-6 in cells primed with LPS alone (Figure S4b). Such results indicate ATP release is at least part of the mechanism transducing Piezo1 channel activation to inhibition of LPS-induced production of TNF-α and IL-6. Treatment with P2 receptor generic antagonist PPADS did not alter, and treatment with P2X7 receptor antagonists slightly increased, the production of TNF-α and IL-6 in BV2 cells exposed with LPS and Yoda1, without effect on the production of TNF-α and IL-6 in cells exposed to LPS alone (Figure S4c–f). These results suggest that P2 receptors including the P2X7 receptor have no or a very limited role in mediating ATP release that transduces Piezo1 channel activation to inhibition of the pro-inflammatory response, raising the question with respect to the role of purinergic signaling evoked by adenosine, one of the major ATP metabolites, through activating the adenosine receptors.

It is well established that more effective production of pro-inflammatory cytokines, particularly IL-1β, in LPS-primed immune cells including microglial cells requires an additional stimulus, such as high concentrations of ATP that is associated with tissue inflammation and damage, which serves as the activation signal to induce sequential activation of the NLRP3 inflammasome and capsase-1 through the P2X7 receptor (Aminzadeh et al., 2018; Monif et al., 2016). Of note, Yoda1-induced Piezo1 channel activation was less effective or ineffective in inhibiting the production of TNF-α and IL-6, as well as IL-1β, in BV2 cells and also in primary microglial cells primed with LPS and subsequently exposed to a high concentration of ATP (Figures S3b and S6d). Given the role of P2X7 receptor activation in LPS-stimulated production of IL-1β, TNF-α, and IL-6 in the presence of high extracellular ATP concentrations, one simple interpretation of these results is that the inhibition by the Piezo1 channel of LPS-induced production of pro-inflammatory cytokines is alleviated by activation of the P2X7 receptor that is associated with tissue inflammation and damage.

In summary, the present study provides evidence to suggest the importance of ATP release and related purinergic signaling in mediating or intervening with Piezo1 channel-dependent inhibition of LPS-induced production of pro-inflammatory cytokines in microglial cells. Clearly, further investigations are needed to better understand the relationships of purinergic signaling and Piezo1 channel signaling in the regulation of the pro-inflammatory function of microglial cells.

4.4 | Piezo1 channel activation reduces LPS-induced NF-κB activation in microglial cells

Intracellular Ca^{2+} signaling has been strongly implicated in regulating various functions of microglial cells, including immune responses (Färber & Kettenmann, 2006; Kettenmann et al., 2011). As discussed above, Piezo1 channel activation mediates Ca^{2+} influx to increase the $[Ca^{2+}]_i$ in both BV2 cells and primary microglial cells. NF-κB and NFAT

are transcription factors known to be activated by intracellular Ca^{2+} signaling and are critical in driving the expression of a range of proteins, including cytokines, in response to a variety of extracellular signals (Dresselhaus & Meffert, 2019; Manocha et al., 2017; Nagamoto-Combs & Combs, 2010; Nguyen et al., 2021). As previously reported in BV2 and N9 microglial cells (Cunha et al., 2016; Jeong et al., 2013), our results showed that exposure to LPS induced phosphorylation of p65, resulting in its nucleus translocation and activation of NF-κB in both BV2 cells and primary microglial cells (Figures 3a–d and 7). Importantly, in both cell types, activation of the Piezo1 channel by Yoda1 significantly attenuated LPS-induced activation and nuclear translocation of p65 (Figures 3a–d and 7). In contrast, exposure to LPS with and without treatment with Yoda1 had no effect on the translocation of NFAT1, a major isoform of NFAT in microglial cells (Manocha et al., 2017; Nagamoto-Combs & Combs, 2010), which was consistently observed in BV2 cells and primary microglial cells (Figure S9). These results support that LPS-induced production of TNF-α and IL-6 is mainly driven by the NF-κB signaling pathway. As shown in BV2 cells, treatment with BAPTA-AM, a widely-used cell-permeant Ca^{2+} chelator, significantly alleviated Yoda1-induced reduction in nuclear translation of NF-κB (Figure 3e,f), suggesting a critical role for Piezo1 channel-mediated Ca^{2+} signaling in inhibiting LPS-induced NF-κB activation. Furthermore, shown in BV2 cells, siRNA-mediated depletion of Piezo1 expression blunted the ability of Yoda1 to inhibit LPS-induced nuclear translation of NF-κB (Figure 4a,b) and, importantly, LPS-induced TNF-α production (Figure 4c). Collectively, these results are consistent with an important role for the Piezo1 channel, particularly Piezo1 channel-mediated Ca^{2+} signaling, in downregulating the pro-inflammatory function of microglial cells by inhibiting the NF-κB signaling pathway.

In this study, we also showed that LPS priming resulted in activation of ERK and p38 in BV2 cells and primary microglial cells (Figure S8a,c) and their inhibition led to reduced production of TNF-α and IL-6 in LPS-primed BV2 cells (Figure 8a,b). These results are in support of a critical role of ERK and p38 in LPS-induced NF-κB activation and production of TNF-α and IL-6 (Figure 9). Treatment with Yoda1 did not significantly alter the activation level of ERK and p38 in LPS-primed microglial cells (Figure S8c,d), suggesting that the Piezo1 channel inhibits LPS-induced activation of NF-κB, and production of TNF-α and IL-6, downstream of ERK or p38.

4.5 | Implications of Piezo1 channel inhibition of microglial pro-inflammatory functions

While the brain is one of the softest tissues in the body, its mechanical properties are dynamic and brain tissues are widely reported to stiffen during development and soften in older age (Budday et al., 2019). Various other factors, particularly pathologically related ones, can also affect the stiffness of local cellular environments in the CNS. Recent studies have reported that chronic mechanical stiffening occurs following spinal cord injury with the formation of a glial scar enmeshed with cross-linked extracellular matrix (Cooper et al., 2020).

Another interesting example is the accumulation and aggregation of amyloid-β (Aβ) peptides, one of the histopathological hallmarks of Alzheimer's disease (AD) that leads to the formation of amyloid plaques that alter the microenvironment of surrounding neurons and glial cells (Calsolaro & Edison, 2016; Mandrekar-Colucci & Landreth, 2010; Meraz-Rios et al., 2013). There is clear evidence that amyloid plaques are considerably stiffer than healthy brain tissue and attract microglial cells via chemo- and duro-taxis (Bollmann et al., 2015; Smith et al., 2006). Emerging evidence from recent studies indicates a potential role for the Piezo1 channel in microglial cells in alleviating the amyloid plaque burden in AD models. For example, in 5xFAD AD mice, treatment with Yoda1 reduced amyloid plaques in the brain, in conjunction with increased localization of microglial cells in the close vicinity of the plaque (Jantti et al., 2022). As shown in the same study, Piezo1 channel-mediated Ca^{2+} signaling in human microglia-like cells derived from inducible pluripotent stem cells was altered by exposure to $Aβ_{42}$, the major neurotoxic amyloid peptide species, which is consistent with the notion that the Piezo1 channel is a previously unrecognized mechanism regulating microglial cell function (Jantti et al., 2022). Another very recent study has demonstrated increased Piezo1 protein expression in microglial cells surrounding amyloid plaques in both 5xFAD mice and human AD patients (Hu et al., 2022). Furthermore, in AD mice, depletion of Piezo1 expression reduced clustering of microglial cells at amyloid plaques and, importantly, treatment with Yoda1 stimulated phagocytosis of Aβ by microglial cells and improved cognitive function (Hu et al., 2022). These results are consistent with our findings, and strongly implicate the Piezo1 channel as an important mechanism regulating microglial cell functions that are critical to the physiological function and pathogenesis of the CNS.

In the present study, the pro-inflammatory phenotype of microglial cells was induced by LPS, a widely used experimental model of inflammation (Batista et al., 2019). There is strong evidence that infection induced by intraperitoneal injection of LPS has significant effects on CNS functions, including upregulation of pro-inflammatory cytokine production in the brain (Püntener et al., 2012; Zhao et al., 2019b), Aβ accumulation (Lee et al., 2008) and increased cognitive deficits (Zhao et al., 2019b). Peripheral bacterial infection upregulates cortical Piezo1 expression in both wild-type and TgF344-AD rats that display increased deposition of amyloid plaques in the brain. Interestingly, Piezo1 upregulation in wild-type rats was primarily neuronal, whereas the increase in Piezo1 expression was mainly localized to reactive astrocytes in AD brains (Velasco-Estevez et al., 2018). These studies indicate that peripheral infection augments CNS inflammation and suggest an interesting relationship between infection-induced inflammation and Piezo1 channel activity in the brain. Further investigations are required to examine the relevance of Piezo1 channel-mediated inhibition of the pro-inflammatory function of microglial cells reported in this study and astrocytes in a recent study (Velasco-Estevez et al., 2020) to the progression of CNS aging, traumatic damage, and neurodegenerative diseases.

In summary, our study provides evidence to show functional expression of the mechanosensitive Piezo1 channel in microglial cells and that activation of the Piezo1 channel leads to intracellular Ca^{2+} signaling that inhibits microglial cell activation and production of pro-inflammatory cytokines, thereby dampening the pro-inflammatory phenotype. Aberrant increase in pro-inflammatory signaling from microglial cells is a crucial pathological factor in brain aging as well as in the pathogenesis of CNS injury and neurodegenerative diseases. Our findings not only provide novel insights into the mechanisms regulating microglial cell functions, but also suggest an interesting therapeutic avenue for restoring the role of microglial cells in protecting and supporting neuronal cell function and reducing neuroinflammation that contributes to neurodegenerative diseases.

AUTHOR CONTRIBUTIONS

Lin-Hua Jiang: conception and design of the research, interpretation of data, and manuscript writing and revision; **Philippa Malko:** conception and design of the research, collection and analysis of data, interpretation of data, and manuscript writing and revision; **Xiaoling Jia:** conception and design of the research; **Ian Wood:** intellectual inputs and manuscript writing and revision. All authors read and approved the final manuscript.

CONFLICT OF INTEREST

The authors declare that they have no conflicting interests to disclose.

DATA AVAILABILITY STATEMENT

The data that support the findings of this study are available from the corresponding author upon reasonable request.

ORCID

Philippa Malko https://orcid.org/0000-0002-5464-806X
Ian Wood https://orcid.org/0000-0003-1886-2533
Lin-Hua Jiang https://orcid.org/0000-0001-6398-0411

REFERENCES

Aminzadeh, M., Roghani, M., Sarfallah, A., & Riazi, G. H. (2018). TRPM2 dependence of ROS-induced NLRP3 activation in Alzheimer's disease. *International Immunopharmacology, 54,* 78–85. https://doi.org/10.1016/j.intimp.2017.10.024

Angelova, D. M., & Brown, D. R. (2019). Microglia and the aging brain: Are senescent microglia the key to neurodegeneration? _Journal of Neurochemistry_, 151(6), 676–688. https://doi.org/10.1111/jnc.14860

Atcha, H., Jairaman, A., Holt, J. R., Meli, V. S., Nagalla, R. R., Veerasubramanian, P. K., Brumm, K. T., Lim, H. E., Othy, S., Cahalan, M. D., Pathak, M. M., & Liu, W. F. (2021). Mechanically activated ion channel Piezo1 modulates macrophage polarization and stiffness sensing. _Nature Communications_, 12(1), 3256. https://doi.org/10.1038/s41467-021-23482-5

Ayata, P., & Schaefer, A. (2020). Innate sensing of mechanical properties of brain tissue by microglia. _Current Opinion in Immunology_, 62, 123–130. https://doi.org/10.1016/j.coi.2020.01.003

Batista, C. R. A., Gomes, G. F., Candelario-Jalil, E., Fiebich, B. L., & de Oliveira, A. C. P. (2019). Lipopolysaccharide-induced neuroinflammation as a bridge to understand neurodegeneration. _International Journal of Molecular Sciences_, 20(9) 2293. https://doi.org/10.3390/ijms20092293

Boche, D., Gerhard, A., Rodriguez-Vieitez, E., & Faculty, M. (2019). Prospects and challenges of imaging neuroinflammation beyond TSPO in Alzheimer's disease. _European Journal of Nuclear Medicine and Molecular Imaging_, 46(13), 2831–2847. https://doi.org/10.1007/s00259-019-04462-w

Bollmann, L., Koser, D. E., Shahapure, R., Gautier, H. O., Holzapfel, G. A., Scarcelli, G., Gather, M. C., Ulbricht, E., & Franze, K. (2015). Microglia mechanics: Immune activation alters traction forces and durotaxis. _Frontiers in Cellular Neuroscience_, 9, 363. https://doi.org/10.3389/fncel.2015.00363

Bruno, L., Karagil, S., Mahmood, A., Elbediwy, A., Stolinski, M., & Mackenzie, F. E. (2021). Mechanosensing and the hippo pathway in microglia: A potential link to Alzheimer's disease pathogenesis? _Cell_, 10(11), 3144. https://doi.org/10.3390/cells10113144

Budday, S., Ovaert, T. C., Holzapfel, G. A., Steinmann, P., & Kuhl, E. (2019). Fifty shades of brain: A review on the mechanical testing and modeling of brain tissue. _Arch. Comput. Methods Eng._, 27(4), 1187–1230. https://doi.org/10.1007/s11831-019-09352-w

Calsolaro, V., & Edison, P. (2016). Neuroinflammation in Alzheimer's disease: Current evidence and future directions. _Alzheimers Dement_, 12 (6), 719–732. https://doi.org/10.1016/j.jalz.2016.02.010

Cinar, E., Zhou, S., DeCourcey, J., Wang, Y., Waugh, R. E., & Wan, J. (2015). Piezo1 regulates mechanotransductive release of ATP from human RBCs. _Proceedings of the National Academy of Sciences of the United States of America_, 112(38), 11783–11788. https://doi.org/10.1073/pnas.1507309112

Cooper, J. G., Sicard, D., Sharma, S., Van Gulden, S., McGuire, T. L., Cajiao, M. P., Tschumperlin, D. J., & Kessler, J. A. (2020). Spinal cord injury results in chronic mechanical stiffening. _Journal of Neurotrauma_, 37(3), 494–506. https://doi.org/10.1089/neu.2019.6540

Coste, B., Mathur, J., Schmidt, M., Earley, T. J., Ranade, S., Petrus, M. J., Dubin, A. E., & Patapoutian, A. (2010). Piezo1 and Piezo2 are essential components of distinct mechanically activated cation channels. _Science_, 330(6000), 55–60. https://doi.org/10.1126/science.1193270

Cunha, C., Gomes, C., Vaz, A. R., & Brites, D. (2016). Exploring new inflammatory biomarkers and pathways during LPS-induced M1 polarization. _Mediators of Inflammation_, 2016, 6986175. https://doi.org/10.1155/2016/6986175

Das, A., Kim, S. H., Arifuzzaman, S., Yoon, T., Chai, J. C., Lee, Y. S., Park, K. S., Jung, K. H., & Chai, Y. G. (2016). Transcriptome sequencing reveals that LPS-triggered transcriptional responses in established microglia BV2 cell lines are poorly representative of primary microglia. _Journal of Neuroinflammation_, 13(1), 182. https://doi.org/10.1186/s12974-016-0644-1

Davalos, D., Grutzendler, J., Yang, G., Kim, J. V., Zuo, Y., Jung, S., Littman, D. R., Dustin, M. L., & Gan, W. B. (2005). ATP mediates rapid microglial response to local brain injury in vivo. _Nature Neuroscience_, 8(6), 752–758. https://doi.org/10.1038/nn1472

Desplat, A., Penalba, V., Gros, E., Parpaite, T., Coste, B., & Delmas, P. (2021). Piezo1-Pannexin1 complex couples force detection to ATP secretion in cholangiocytes. _The Journal of General Physiology_, 153(12), e202112871. https://doi.org/10.1085/jgp.202112871

Diem, K., Fauler, M., Fois, G., Hellmann, A., Winokurow, N., Schumacher, S., Kranz, C., & Frick, M. (2020). Mechanical stretch activates Piezo1 in caveolae of alveolar type I cells to trigger ATP release and paracrine stimulation of surfactant secretion from alveolar type II cells. _The FASEB Journal_, 34(9), 12785–12804. https://doi.org/10.1096/fj.202000613RRR

Dresselhaus, E. C., & Meffert, M. K. (2019). Cellular specificity of NF-κB function in the nervous system. _Frontiers in Immunology_, 10, 1043. https://doi.org/10.3389/fimmu.2019.01043

Durham, B. S., Grigg, R., & Wood, I. C. (2017). Inhibition of histone deacetylase 1 or 2 reduces induced cytokine expression in microglia through a protein synthesis independent mechanism. _Journal of Neurochemistry_, 143(2), 214–224. https://doi.org/10.1111/jnc.14144

Fang, X. Z., Zhou, T., Xu, J. Q., Wang, Y. X., Sun, M. M., He, Y. J., Pan, S. W., Xiong, W., Peng, Z. K., Gao, X. H., & Shang, Y. (2021). Structure, kinetic properties and biological function of mechanosensitive piezo channels. _Cell & Bioscience_, 11(1), 13. https://doi.org/10.1186/s13578-020-00522-z

Färber, K., & Kettenmann, H. (2006). Purinergic signaling and microglia. _Pflügers Archiv_, 452(5), 615–621. https://doi.org/10.1007/s00424-006-0064-7

Fields, R. D., & Burnstock, G. (2006). Purinergic signalling in neuron-glia interactions. _Nature Reviews. Neuroscience_, 7(6), 423–436. https://doi.org/10.1038/nrn1928

Gudipaty, S. A., Lindblom, J., Loftus, P. D., Redd, M. J., Edes, K., Davey, C. F., Krishnegowda, V., & Rosenblatt, J. (2017). Mechanical stretch triggers rapid epithelial cell division through Piezo1. _Nature_, 543(7643), 118–121. https://doi.org/10.1038/nature21407

He, Y., Yao, X., Taylor, N., Bai, Y., Lovenberg, T., & Bhattacharya, A. (2018). RNA sequencing analysis reveals quiescent microglia isolation methods from postnatal mouse brains and limitations of BV2 cells. _Journal of Neuroinflammation_, 15(1), 153. https://doi.org/10.1186/s12974-018-1195-4

Hu, J., Chen, Q., Zhu, H., Hou, L., Liu, W., Yang, Q., Shen, H., Chai, G., Zhang, B., Chen, S., Cai, Z., Wu, C., Hong, F., Li, H., Chen, S., Xiao, N., Wang, Z.X., Zhang, X., Wang, B., & Mo, W. (2022). Microglial Piezo1 senses Aβ fibrils stiffness to restrict Alzheimer's disease. _Neuron_, https://doi.org/10.1016/j.neuron.2022.10.021

Jantti, H., Sitnikova, V., Ishchenko, Y., Shakirzyanova, A., Giudice, L., Ugidos, I. F., Gomez-Budia, M., Korvenlaita, N., Ohtonen, S., Belaya, I., Fazaludeen, F., Mikhailov, N., Gotkiewicz, M., Ketola, K., Lehtonen, S., Koistinaho, J., Kanninen, K. M., Hernandez, D., Pebay, A., & Malm, T. (2022). Microglial amyloid beta clearance is driven by PIEZO1 channels. _Journal of Neuroinflammation_, 19(1), 147. https://doi.org/10.1186/s12974-022-02486-y

Jeong, J. W., Lee, W. S., Shin, S. C., Kim, G. Y., Choi, B. T., & Choi, Y. H. (2013). Anthocyanins downregulate lipopolysaccharide-induced inflammatory responses in BV2 microglial cells by suppressing the NF-κB and Akt/MAPKs signaling pathways. _International Journal of Molecular Sciences_, 14(1), 1502–1515. https://doi.org/10.3390/ijms14011502

Kettenmann, H., Hanisch, U. K., Noda, M., & Verkhratsky, A. (2011). Physiology of microglia. _Physiological Reviews_, 91(2), 461–553. https://doi.org/10.1152/physrev.00011.2010

Lannes, N., Eppler, E., Etemad, S., Yotovski, P., & Filgueira, L. (2017). Microglia at center stage: A comprehensive review about the versatile and unique residential macrophages of the central nervous system. _Oncotarget_, 8(69), 114393–114413. https://doi.org/10.18632/oncotarget.23106

Lee, J. W., Lee, Y. K., Yuk, D. Y., Choi, D. Y., Ban, S. B., Oh, K. W., & Hong, J. T. (2008). Neuro-inflammation induced by lipopolysaccharide causes cognitive impairment through enhancement of beta-amyloid generation. _Journal of Neuroinflammation_, 5, 37. https://doi.org/10.1186/1742-2094-5-37

Leng, F., & Edison, P. (2021). Neuroinflammation and microglial activation in Alzheimer disease: Where do we go from here? *Nature Reviews. Neurology*, *17*(3), 157–172. https://doi.org/10.1038/s41582-020-00435-y

Liu, H., Bian, W., Yang, D., Yang, M., & Luo, H. (2021). Inhibiting the Piezo1 channel protects microglia from acute hyperglycaemia damage through the JNK1 and mTOR signalling pathways. *Life Sciences*, *264*, 118667. https://doi.org/10.1016/j.lfs.2020.118667

Liu, Y., Wu, X. M., Luo, Q. Q., Huang, S., Yang, Q. W., Wang, F. X., Ke, Y., & Qian, Z. M. (2015). CX3CL1/CX3CR1-mediated microglia activation plays a detrimental role in ischemic mice brain via p38MAPK/PKC pathway. *Journal of Cerebral Blood Flow and Metabolism*, *35*(10), 1623–1631. https://doi.org/10.1038/jcbfm.2015.97

Livak, K. J., & Schmittgen, T. D. (2001). Analysis of relative gene expression data using real-time quantitative PCR and the 2(-Delta Delta C(T)) method. *Methods*, *25*(4), 402–408. https://doi.org/10.1006/meth.2001.1262

Luan, W., Li, M., Wu, C., Shen, X., & Sun, Z. (2022). Proteomic dissimilarities of primary microglia and BV2 cells under stimuli. *The European Journal of Neuroscience*, *55*(7), 1709–1723. https://doi.org/10.1111/ejn.15637

Luca, A., Calandra, C., & Luca, M. (2018). Molecular bases of Alzheimer's disease and neurodegeneration: The role of neuroglia. *Aging and Disease*, *9*(6), 1134–1152. https://doi.org/10.14336/AD.2018.0201

Mandrekar-Colucci, S., & Landreth, G. E. (2010). Microglia and inflammation in Alzheimer's disease. *CNS & Neurological Disorders Drug Targets*, *9*(2), 156–167. https://doi.org/10.2174/187152710791012071

Manocha, G. D., Ghatak, A., Puig, K. L., Kraner, S. D., Norris, C. M., & Combs, C. K. (2017). NFATc2 modulates microglial activation in the AβPP/PS1 mouse model of Alzheimer's disease. *Journal of Alzheimer's Disease*, *58*(3), 775–787. https://doi.org/10.3233/JAD-151203

McHugh, B. J., Buttery, R., Lad, Y., Banks, S., Haslett, C., & Sethi, T. (2010). Integrin activation by Fam38A uses a novel mechanism of R-Ras targeting to the endoplasmic reticulum. *Journal of Cell Science*, *123*(Pt 1), 51–61. https://doi.org/10.1242/jcs.056424

Meraz-Rios, M. A., Toral-Rios, D., Franco-Bocanegra, D., Villeda-Hernandez, J., & Campos-Pena, V. (2013). Inflammatory process in Alzheimer's disease. *Frontiers in Integrative Neuroscience*, *7*, 59. https://doi.org/10.3389/fnint.2013.00059

Miyamoto, T., Mochizuki, T., Nakagomi, H., Kira, S., Watanabe, M., Takayama, Y., Suzuki, Y., Koizumi, S., Takeda, M., & Tominaga, M. (2014). Functional role for Piezo1 in stretch-evoked Ca^{2+} influx and ATP release in urothelial cell cultures. *The Journal of Biological Chemistry*, *289*(23), 16565–16575. https://doi.org/10.1074/jbc.M113.528638

Momin, A., Bahrampour, S., Min, H. K., Chen, X., Wang, X., Sun, Y., & Huang, X. (2021). Channeling force in the brain: Mechanosensitive ion channels choreograph mechanics and malignancies. *Trends in Pharmacological Sciences*, *42*(5), 367–384. https://doi.org/10.1016/j.tips.2021.02.006

Monif, M., Reid, C. A., Powell, K. L., Drummond, K. J., O'Brien, T. J., & Williams, D. A. (2016). Interleukin-1β has trophic effects in microglia and its release is mediated by P2X7R pore. *Journal of Neuroinflammation*, *13*(1), 173. https://doi.org/10.1186/s12974-016-0621-8

Moon, D. O., Kim, K. C., Jin, C. Y., Han, M. H., Park, C., Lee, K. J., Park, Y. M., Choi, Y. H., & Kim, G. Y. (2007). Inhibitory effects of eicosapentaenoic acid on lipopolysaccharide-induced activation in BV2 microglia. *International Immunopharmacology*, *7*(2), 222–229. https://doi.org/10.1016/j.intimp.2006.10.001

Moraes, C. A., Santos, G., de Sampaio e Spohr, T. C., D'Avila, J. C., Lima, F. R., Benjamim, C. F., Bozza, F. A., & Gomes, F. C. (2015). Activated microglia-induced deficits in excitatory synapses through IL-1β: Implications for cognitive impairment in sepsis. *Molecular Neurobiology*, *52*(1), 653–663. https://doi.org/10.1007/s12035-014-8868-5

Mousawi, F., Peng, H., Li, J., Ponnambalam, S., Roger, S., Zhao, H., Yang, X., & Jiang, L. H. (2020). Chemical activation of the Piezo1 channel drives mesenchymal stem cell migration via inducing ATP release and activation of P2 receptor purinergic signaling. *Stem Cells*, *38*(3), 410–421. https://doi.org/10.1002/stem.3114

Nagamoto-Combs, K., & Combs, C. K. (2010). Microglial phenotype is regulated by activity of the transcription factor, NFAT (nuclear factor of activated T cells). *The Journal of Neuroscience*, *30*(28), 9641–9646. https://doi.org/10.1523/jneurosci.0828-10.2010

Nguyen, P. L., Bui, B. P., Duong, M. T. H., Lee, K., Ahn, H. C., & Cho, J. (2021). Suppression of LPS-induced inflammation and cell migration by azelastine through inhibition of JNK/NF-κB pathway in BV2 microglial cells. *International Journal of Molecular Sciences*, *22*(16). 9061. https://doi.org/10.3390/ijms22169061

North, R. A., & Surprenant, A. (2000). Pharmacology of cloned P2X receptors. *Annual Review of Pharmacology and Toxicology*, *40*, 563–580. https://doi.org/10.1146/annurev.pharmtox.40.1.563

Noursadeghi, M., Tsang, J., Haustein, T., Miller, R. F., Chain, B. M., & Katz, D. R. (2008). Quantitative imaging assay for NF-κB nuclear translocation in primary human macrophages. *Journal of Immunological Methods*, *329*(1–2), 194–200. https://doi.org/10.1016/j.jim.2007.10.015

Orihuela, R., McPherson, C. A., & Harry, G. J. (2016). Microglial M1/M2 polarization and metabolic states. *British Journal of Pharmacology*, *173*(4), 649–665. https://doi.org/10.1111/bph.13139

Pathak, M. M., Nourse, J. L., Tran, T., Hwe, J., Arulmoli, J., Le, D. T., Bernardis, E., Flanagan, L. A., & Tombola, F. (2014). Stretch-activated ion channel Piezo1 directs lineage choice in human neural stem cells. *Proceedings of the National Academy of Sciences of the United States of America*, *111*(45), 16148–16153. https://doi.org/10.1073/pnas.1409802111

Pelegrin, P. (2021). P2X7 receptor and the NLRP3 inflammasome: Partners in crime. *Biochemical Pharmacology*, *187*, 114385. https://doi.org/10.1016/j.bcp.2020.114385

Pena-Ortega, F. (2017). Pharmacological tools to activate microglia and their possible use to study neural network patho-physiology. *Current Neuropharmacology*, *15*(4), 595–619. https://doi.org/10.2174/1570159x14666160928151546

Plotnikov, A., Zehorai, E., Procaccia, S., & Seger, R. (2011). The MAPK cascades: Signaling components, nuclear roles and mechanisms of nuclear translocation. Biochimica et Biophysica Acta (BBA) - molecular. *Cell Research*, *1813*(9), 1619–1633. https://doi.org/10.1016/j.bbamcr.2010.12.012

Püntener, U., Booth, S. G., Perry, V. H., & Teeling, J. L. (2012). Long-term impact of systemic bacterial infection on the cerebral vasculature and microglia. *Journal of Neuroinflammation*, *9*(1), 146. https://doi.org/10.1186/1742-2094-9-146

Santa-Cecília, F. V., Socias, B., Ouidja, M. O., Sepulveda-Diaz, J. E., Acuña, L., Silva, R. L., Michel, P. P., Del-Bel, E., Cunha, T. M., & Raisman-Vozari, R. (2016). Doxycycline suppresses microglial activation by inhibiting the p38 MAPK and NF-κB signaling pathways. *Neurotoxicity Research*, *29*(4), 447–459. https://doi.org/10.1007/s12640-015-9592-2

Sims, R., van der Lee, S. J., Naj, A. C., Bellenguez, C., Badarinarayan, N., Jakobsdottir, J., Kunkle, B. W., Boland, A., Raybould, R., Bis, J. C., Martin, E. R., Grenier-Boley, B., Heilmann-Heimbach, S., Chouraki, V., Kuzma, A. B., Sleegers, K., Vronskaya, M., Ruiz, A., Graham, R. R., & Schellenberg, G. D. (2017). Rare coding variants in PLCG2, ABI3, and TREM2 implicate microglial-mediated innate immunity in Alzheimer's disease. *Nature Genetics*, *49*(9), 1373–1384. https://doi.org/10.1038/ng.3916

Smith, J. F., Knowles, T. P., Dobson, C. M., Macphee, C. E., & Welland, M. E. (2006). Characterization of the nanoscale properties of individual amyloid fibrils. *Proceedings of the National Academy of Sciences of the United States of America*, *103*(43), 15806–15811. https://doi.org/10.1073/pnas.0604035103

Solis, A. G., Bielecki, P., Steach, H. R., Sharma, L., Harman, C. C. D., Yun, S., de Zoete, M. R., Warnock, J. N., To, S. D. F., York, A. G., Mack, M.,

Schwartz, M. A., Dela Cruz, C. S., Palm, N. W., Jackson, R., & Flavell, R. A. (2019). Mechanosensation of cyclical force by PIEZO1 is essential for innate immunity. *Nature*, *573*(7772), 69–74. https://doi.org/10.1038/s41586-019-1485-8

Soltys, Z., Ziaja, M., Pawlinski, R., Setkowicz, Z., & Janeczko, K. (2001). Morphology of reactive microglia in the injured cerebral cortex. Fractal analysis and complementary quantitative methods. *Journal of Neuroscience Research*, *63*(1), 90–97. https://doi.org/10.1002/1097-4547(20010101)63:1<90::AID-JNR11>3.0.CO;2-9

Song, Y., Li, D., Farrelly, O., Miles, L., Li, F., Kim, S. E., Lo, T. Y., Wang, F., Li, T., Thompson-Peer, K. L., Gong, J., Murthy, S. E., Coste, B., Yakubovich, N., Patapoutian, A., Xiang, Y., Rompolas, P., Jan, L. Y., & Jan, Y. N. (2019). The mechanosensitive ion channel piezo inhibits axon regeneration. *Neuron*, *102*(2), 373–389. https://doi.org/10.1016/j.neuron.2019.01.050

Sun, X. F., Qiao, W. W., Meng, L. Y., & Bian, Z. (2022). PIEZO1 ion channels mediate mechanotransduction in odontoblasts. *Journal of Endodontia*, *48*(6), 749–758. https://doi.org/10.1016/j.joen.2022.02.005

Sun, Y., Leng, P., Song, M., Li, D., Guo, P., Xu, X., Gao, H., Li, Z., Li, C., & Zhang, H. (2020). Piezo1 activates the NLRP3 inflammasome in nucleus pulposus cell-mediated by Ca(2+)/NF-κB pathway. *International Immunopharmacology*, *85*, 106681. https://doi.org/10.1016/j.intimp.2020.106681

Syeda, R., Xu, J., Dubin, A. E., Coste, B., Mathur, J., Huynh, T., Matzen, J., Lao, J., Tully, D. C., Engels, I. H., Petrassi, H. M., Schumacher, A. M., Montal, M., Bandell, M., & Patapoutian, A. (2015). Chemical activation of the mechanotransduction channel Piezo1. *eLife*, *4*, e07369. https://doi.org/10.7554/eLife.07369

Szepesi, Z., Manouchehrian, O., Bachiller, S., & Deierborg, T. (2018). Bidirectional microglia-neuron communication in health and disease. *Frontiers in Cellular Neuroscience*, *12*(323), 323. https://doi.org/10.3389/fncel.2018.00323

Velasco-Estevez, M., Mampay, M., Boutin, H., Chaney, A., Warn, P., Sharp, A., Burgess, E., Moeendarbary, E., Dev, K. K., & Sheridan, G. K. (2018). Infection augments expression of mechanosensing Piezo1 channels in amyloid plaque-reactive astrocytes. *Frontiers in Aging Neuroscience*, *10*, 332. https://doi.org/10.3389/fnagi.2018.00332

Velasco-Estevez, M., Rolle, S. O., Mampay, M., Dev, K. K., & Sheridan, G. K. (2020). Piezo1 regulates calcium oscillations and cytokine release from astrocytes. *Glia*, *68*(1), 145–160. https://doi.org/10.1002/glia.23709

Wang, S., Chennupati, R., Kaur, H., Iring, A., Wettschureck, N., & Offermanns, S. (2016). Endothelial cation channel PIEZO1 controls blood pressure by mediating flow-induced ATP release. *The Journal of Clinical Investigation*, *126*(12), 4527–4536. https://doi.org/10.1172/JCI87343

Wang, Y., & Xiao, B. (2018). The mechanosensitive Piezo1 channel: Structural features and molecular bases underlying its ion permeation and mechanotransduction. *The Journal of Physiology*, *596*(6), 969–978. https://doi.org/10.1113/JP274404

Wei, L., Mousawi, F., Li, D., Roger, S., Li, J., Yang, X., & Jiang, L. H. (2019). Adenosine triphosphate release and P2 receptor signaling in Piezo1 channel-dependent mechanoregulation. *Frontiers in Pharmacology*, *10*, 1304. https://doi.org/10.3389/fphar.2019.01304

Wei, Y., Chen, T., Bosco, D. B., Xie, M., Zheng, J., Dheer, A., Ying, Y., Wu, Q., Lennon, V. A., & Wu, L. J. (2021). The complement C3-C3aR pathway mediates microglia-astrocyte interaction following status epilepticus. *Glia*, *69*(5), 1155–1169. https://doi.org/10.1002/glia.23955

Wolf, S. A., Boddeke, H. W., & Kettenmann, H. (2017). Microglia in physiology and disease. *Annual Review of Physiology*, *79*, 619–643. https://doi.org/10.1146/annurev-physiol-022516-034406

Zanier, E. R., Fumagalli, S., Perego, C., Pischiutta, F., & De Simoni, M. G. (2015). Shape descriptors of the "never resting" microglia in three different acute brain injury models in mice. *Intensive Care Medicine Experimental*, *3*(1), 39. https://doi.org/10.1186/s40635-015-0039-0

Zhao, C., Sun, Q., Tang, L., Cao, Y., Nourse, J. L., Pathak, M. M., Lu, X., & Yang, Q. (2019). Mechanosensitive ion channel piezo1 regulates diet-induced adipose inflammation and systemic insulin resistance. *Frontiers in Endocrinology*, *10*, 373. https://doi.org/10.3389/fendo.2019.00373

Zhao, J., Bi, W., Xiao, S., Lan, X., Cheng, X., Zhang, J., Lu, D., Wei, W., Wang, Y., Li, H., Fu, Y., & Zhu, L. (2019). Neuroinflammation induced by lipopolysaccharide causes cognitive impairment in mice. *Scientific Reports*, *9*(1), 5790. https://doi.org/10.1038/s41598-019-42286-8

Zhou, T., Gao, B., Fan, Y., Liu, Y., Feng, S., Cong, Q., Zhang, X., Zhou, Y., Yadav, P. S., Lin, J., Wu, N., Zhao, L., Huang, D., Zhou, S., Su, P., & Yang, Y. (2020). Piezo1/2 mediate mechanotransduction essential for bone formation through concerted activation of NFAT-YAP1-ß-catenin. *eLife*, *9*, e52779. https://doi.org/10.7554/eLife.52779

SUPPORTING INFORMATION

Additional supporting information can be found online in the Supporting Information section at the end of this article.